Atacama
Large
Millimeter /
submillimeter
Array

Band-to-band Phase Transfer with ALMA: April-May 2013

ALMA Technical Note Number: 1

Status: FINAL

Prepared by:	**Organization:**	**Date:**
Kim Scott	NAASC	27 May 2013

Band-to-band Phase Transfer with ALMA: April-May 2013

Kim Scott

May 27 2013

1 Introduction

Finding strong calibrators within 10° of a science target at frequencies above $\sim 300\,\mathrm{GHz}$ is challenging. Using a phase calibrator further away is undesirable, since both systematic phase errors that arise from antenna position uncertainties and variable tropospheric delays get worse. Quasars are much brighter at lower frequencies, and so we would like to be able to observe a quasar within 10° of a science target at a lower frequency, and correct its phase to that of the target frequency. In this report, I describe initial testing of band-to-band phase transfer (BBPT). More information is given in the ALMA JIRA ticket CSV-2730.

This report is organized as follows: in Section 2, I describe the basic method of BBPT; in Section 3, I discuss the commissioning tests carried out in April and May 2013; I discuss the data reduction steps to analyze these data in Section 4, and present the main results from this study in Section 5; I summarize this work in Section 6.

2 Band-to-band Phase Transfer: General Description of the Method

The observed phase difference between interferometric observations at two different frequencies (ν_1, ν_2) has two components. The first is an instrumental phase difference that is almost constant in time ($\phi_i(\nu_1)$, $\phi_i(\nu_2)$), and the second is a highly variable delay component due to tropospheric fluctuations ($\phi_t(\nu_1, t)$, $\phi_t(\nu_2, t)$). The latter thus scales with frequency, such that

$$\phi_t(\nu_2, t) = \frac{\nu_2}{\nu_1} \times \phi_t(\nu_1, t). \tag{1}$$

We need a calibration sequence that allows us to solve for both types. The basic method is to observe a bright quasar (BQ) that is $> 10°$ from the science target (ST) at both frequencies in order to measure the instrumental phase difference, and then observe a fainter

quasar (FQ) $< 10^{o}$ from the target at the lower frequency to track the delay component with time. The scan sequence looks like this:

1. BQ(ν_1)
2. BQ(ν_2)
3. FQ(ν_1)
4. ST(ν_2)
5. Repeat steps 3 and 4 for time $t_{\rm crit}$
6. FQ(ν_1)
7. Repeat all steps to the end of the execution.

The BQ(ν_1) – BQ(ν_2) scan pairs are revisited every $t_{\rm crit}$ minutes (hours?) to track the (hopefully) small drifts in instrumental phase differences. Determining an optimal value of $t_{\rm crit}$ is one of our goals. Another important scale is the time it takes to switch between frequencies, $t_{\rm switch}$. This must be short enough that tropospheric variations between adjacent scans at different frequencies are small, so that the phase difference between the BQ(ν_1) – BQ(ν_2) scan pairs is dominated by the constant instrumental phase difference.

3 Commissioning Tests, April-May 2013

We carried out a number of BBPT tests at ALMA during commissioning time in April and May 2013. These include testing BBPT between Bands 3 (90 GHz) and 7 (340 GHz), and Bands 6 (240 GHz) and 9 (690 GHz). For these initial tests, we observe a single quasar, and simply swtich between the two frequencies. These data thus are not able to inform on the degradation of the phase transfer from one source to another, which we will test in the future. All data were taken in TDM mode. Table 1 summarizes the BBPT tests carried out during these observing sessions. Some of the executions were run back-to-back using similar settings; for these, I concatenate the data for the analysis as noted in Table 1.

Since we only observed a single source per execution, I select a finite number of adjacent low/high frequency scan pairs to treat as the "BQ" scans, which I use to solve for the instrumental phase difference (see Section 4). I select scan pairs at the beginning, middle, and end of the executions to be approximately equally separated in time by $t_{\rm crit} \approx 10$ min. The rest of the scans I treat as the "FQ" (low frequency) and "ST" (high frequency) observations, using the low frequency observations to derive a phase solution to apply to the high frequency observations.

The BBPT script includes on option to use the scan-sequencing mode, which allows the user to specify a list of scan-level observations to be queued in the correlator. This is desirable for BBPT to reduce the time lag between observations at the two frequencies. An

additional option with this mode is pre-tuning of the LO settings. We ran several BBPT tests with and without scan-sequencing, including one test data-set with pre-tuning. With scan-sequencing and no pre-tuning of the LO's, this reduced the time to switch between frequencies from $t_{\rm switch} = 34\,{\rm s}$ to 29 s. With pre-tuning $t_{\rm switch}$ is reduced to 10 s. The values for $t_{\rm switch}$ for all executions are shown in Table 1, with the ones that used scan-sequencing and/or pre-tuning indicated.

At this time, the observations must be run in script mode (implementation of this observing mode into scheduling blocks is in progress). It is difficult to include $T_{\rm sys}$ measurements in script mode unless they are done after *every* delay scan, which introduces an additional time lag of $\sim 20\,{\rm s}$ between adjacent observations at different frequencies. This can hinder the ability to calibrate out the instrumental phase differences. We decided to remove the $T_{\rm sys}$ measurements for the second half of the executions (see Table 1). The resulting time lag between adjacent scans ranges from $t_{\rm switch} = 10\,{\rm s}$ to 50 s, as listed in Table 1.

Without $T_{\rm sys}$ measurements, I am thus only testing phase calibration, and not amplitude calibration (which we'll want to do at some point). The observations include water vapor radiometer (WVR) measurments, so I applied the WVR calibration to all data. Since we observe a bright quasar, I use all scans to determine a bandpass solution.

4 Data Reduction

I reduce each observation using the same procedure. The main steps are listed below. All of this analyis was done using CASA version 4.0.1.

1. Flag autocorrelations, and $T_{\rm sys}$ scans (if present).
2. **wvrgcal**, and smooth calibration to 2 s. Apply WVR calibration table to data and split out science spws (four in each band).
3. Flag shadowed antennas and edge channels. Inspect data with **plotms** and flag other bad antennas, scans, etc.
4. Bandpass calibration:
   (a) **gaincal** with solint='int' to determine phase solutions on integration time scales.
   (b) **bandpass** with solint='inf' and combine='scan' to use all scans in determining the bandpass for each spw, applying gain table above on-the-fly. This bandpass calibration table is applied on-the-fly in all calls to **gaincal** below.
5. Gain calibration:
   (a) Run **gaincal** to derive the instrumental phase offset between the two bands using selected adjacent scan pairs at the beginning, middle, and end of the observation, such that $t_{\rm crit} \sim 10\,{\rm min}$.

(b) Run **gaincal** to derive the phase solutions for all of the low frequency scans. Apply the calibration table from the previous step on-the-fly to remove the instrumental phase component before solving. Since this also removes offsets between the spws and polarizations, I use combine='spw' and gaintype='T' in this step to increase the signal-to-noise.

(c) Apply both calibration tables to the high frequency data. The first removes the instrumental phase component. For the second, the phase table determined from the low frequency data is applied to the high frequency data via spwmap. The interp='linearPD' option in **gaincal** scales the low frequency solutions to the high frequency data by the ratio of the frequencies (Equation 1).

Step 5 is demonstrated in Figures 1, 2, and 3. For this study, I examine both 1) applying the low frequency phase gain tables to the high frequency data *without* scaling by the frequency ratio (interp='linear') and 2) applying them with scaling (interp='linearPD').

5 Results

5.1 Initial Checks

I did several important checks that I don't describe in detail here, but I want to briefly mention.

First, I tested whether the phases in the four spws (and two polarizations) within a given band track each other well. That is, while they may be offset by a constant value, they follow the same trend about this mean offset as a function of time. This is expected since these variations are due to tropopheric fluctuations which depend on frequency. I found that the spws within a given band do indeed trace each other well (this has also been studied by others and reported in the previous JIRA ticket on BBPT (CSV-413).

In previous analyses (see CSV-413) it was reported that interp='linearPD' was not scaling the phases by the frequency ratio in some cases. I investigated this since we want to make sure that this option is working at the task level in CASA. I tested this by comparing the phase solutions from **gaincal** using interp='linearPD', and using interp='linear', where for the latter, I scaled the solutions manually using the CASA table tools. These give the same results, confirming that interp='linearPD' scales by frequency as expected. The previous reports that this was not working may have been due to errors in using spwmap to apply solutions from one band to another.

5.2 Main Results

In Figure 3, I compare the corrected phases after **applycal** for one of the data-sets and a single antenna, using Band 3 to calibrate Band 7, and using Band 7 to calibrate Band 7. The latter is a self-cal and is used as a control case to evaluate the effects of calibrating the high frequency data with low frequency gain solutions. There are two main effects that will

degrade the final image quality: 1) a mean non-zero phase offset will result in positional errors, and 2) an increase in the corrected phase r.m.s. will spread out the signal in the image plane. I therefore try to boil down these results from all data-sets and all baselines by looking at the mean and standard deviation per antenna. I focus on baselines shorter than 400 m here since there are very few data points at longer baselines.

Figures 4 to 12 show the mean corrected phase for each antenna as a function of baseline distance for the nine Band 3/Band 7 observations, using interp='linear' (i.e. not scaling the solutions by the frequency ratio). The error bars show the corrected phase r.m.s. The results are summarized in Table 2. Each antenna shows a mean phase offset ranging (in absolute value) from $\sim 2{-}20^{\rm o}$ which tends to be larger for the longer baselines (but not always); however, the phase offset averaged over all antennas is $< 5^{\rm o}$. Table 2 also shows the mean (and range of) phase r.m.s., which is displayed as a function of baseline distance for all observations in Figure 13. The phase r.m.s. ranges from $\sim 2 - 20^{\rm o}$ and tends to increase with baseline distance. It is interesting to compare this with the phase r.m.s. for the control case (self-calibrating the Band 7 data): the fractional increase in the r.m.s. over the self-cal r.m.s. is also given in Table 2 and shown as a function of baseline distance in Figure 14. There is a wide range of values in the fractional r.m.s. increase over all observations (25% to 400%) with no obvious correlation with weather conditions (PWV), though these may be dominated by a few outliers. The next step will be to continue with the imaging steps and evaluate how much these effects degrade the image quality (positional errors, peak flux attenuation, etc.).

The results for the Band 3/Band 7 observations using interp='linearPD' – where the phase solutions in Band 3 are scaled by the frequency ratio and then applied to the Band 7 data – are shown in Figures 15 to 25 and summarized in Table 3. I find that the phase r.m.s. is similar (slightly higher) to that seen without frequency scaling; however, the mean corrected phases are generally higher (i.e. worse). It is not clear why this is the case and this needs to be investigated further. With frequency scaling ($\nu_{B7}/\nu_{B3} = 3.9$ in this case), any error in measuring the instrumental phase offset between the two bands will propagate. It's possible that the results we are seeing imply that values of $t_{\rm switch}$ = 10-50 s are not fast enough to remove the effects of tropospheric fluctuations. It is interesting to note that for the one data-set where scan sequencing and pre-tuning of the LO was used (X3a+X6b) – where $t_{\rm switch}$ is only 10 s – the phase transfer was not improved. I also tried calibrating out the phase offset using an average over the whole execution for Xc87, with the idea that this could help average out atmospheric fluctuations, but this did not improve the observed phase scatter.

The results for the Band 6/Band 9 observations using interp='linear' are shown in Figures 26 to 30 and summarized in Table 4; the results using interp='linearPD' are shown in Figures 31 to 35 and summarized in Table 5. For interp='linear', we see mean phase offsets similar to those observed for the Band 3/Band 7 data (absolute values up to $\sim 20^{\rm o}$), but the mean over all antennas is $\lesssim 1^{\rm o}$. Again, there is a large range in the fractional increase in the phase r.m.s., particularly for the X33+X66 observation. We see the same effect as with the Band 3/Band 7 data-sets, where using interp='linearPD' results in slightly higher phase

r.m.s. and larger mean offsets.

5.3 Other Tests

I did a few additional tests that I won't present in detail, but will mention here.

I used one of the data-sets (Band 3 to Band 7) to verify that applying the WVR corrections improves BBPT. I find that the phase r.m.s. in the Band 7 data after applying the Band 3 gain table is indeed lower when the WVR corrections are applied to both bands. There are some scans for which the WVR corrections make the phases considerably worse. These seem to occur at random times. I flag such scans in my analysis above.

I did some moderate testing of changing the value of $t_{\rm crit}$ for Xc87, varying between $\sim$ 5-25 min, to see if the mean corrected phases and r.m.s decrease with smaller values. The value of $t_{\rm crit}$ did not make any difference.

Finally, mathematically speaking, Steps 5a and 5b can be reversed – that is, one can first derive the low frequency phase solutions, then use adjacent scan pairs in both frequencies to derive the phase offset. I tested both methods and find that they give similar results. However, the method described in Section 4 allows us to combine spectral windows and polarizations and increase the signal to noise, so I chose this one.

6 Conclusions and Future Tests

The main results from these test data are:

1. The observed phases in the four spws and two polarizations track each other very well, and can thus be combined after running **gaincal** on a subset of the scans to increase the signal-to-noise. This is good, since in principle we will be able to choose relatively weak phase calibrators (even in Band 3) that are spatially close to the target of interest for BBPT.

2. Using interp='linearPD' in **applycal** scales the phase gains by the ratio of the frequencies in the two bands, as expected. This is in contrast to (some) previous tests, which were likely using spwmap to transfer the phases at one spw to another incorrectly.

3. For both Band 3/Band 7 and Band 6/Band 9 BBPT tests, we see mean corrected phases from $\sim$ 2-20%, with phase r.m.s. that increases with baseline distance. The next step is to image the high frequency data to determine the overall effect on the image quality.

4. Using interp='linearPD' to scale the low frequency phase solutions to high frequency in general gives worse results, which is opposite from what we expect. This could mean that switching times between the two frequencies of < 10 s are needed. However, we have only a single data-set with $t_{\rm switch} \lesssim 30$ s, which was executed after a major power disruption at the site, and the system had been brought back up without full testing

of the antennas, correlator, etc. It may be worth doing a few more executions with scan sequencing and pre-tuning of the LO to get more data with short $t_{\rm switch}$.

Very few of the observations had baselines $> 400\,$m, so I have focused on the phase transfer on smaller baselines. The few data-sets with longer baselines show that they follow the general trend of increasing residual phase r.m.s. with baseline distance. BBPT on longer baselines may be challenging, and we will need more data to test this.

Table 1: Band-to-band Phase Transfer Data: April-May 2013

Date	ASDM Name	Bands	Source	N_{ant}	PWV (mm)	$t_{\rm switch}$ (s)	scanSeq?	pre-tune LO?
17-Apr-2013	uid___A002_X61068c_Xc87	3/7	3c279	26	1.1	51	no	no
21-Apr-2013	uid___A002_X617ed5_X12	3/7	3c279	32	1.2	52	no	no
21-Apr-2013	uid___A002_X617ed5_X4a5	3/7	1924-292	30	1.2	51	no	no
21-Apr-2013	uid___A002_X616da1_X530	3/7	3c279	29	1.1	53	no	no
21-Apr-2013	uid___A002_X616da1_X717	3/7	3c279	29	1.1	53	no	no
22-Apr-2013	uid___A002_X618902_X129	3/7	3c279	30	1.2	40	no	no
08-May-2013	uid___A002_X62932c_X358	3/7	1924-292	20	0.45	34	no	no
08-May-2013	uid___A002_X62932c_X2f6	3/7	1924-292	20	0.42	29	yes	no
	uid___A002_X62932c_X327[b]							
10-May-2013	uid___A002_X62cc28_X3a	3/7	3c279	16	1.05	10	yes	yes
	uid___A002_X62cc28_X6b[b]							
08-May-2013	uid___A002_X62932c_X1c5	6/9	1924-292	26	0.45	34	no	no
	uid___A002_X62932c_X202[b]							
08-May-2013	uid___A002_X62932c_X6e	6/9	1924-292	27	0.49	29	yes	no
	uid___A002_X62932c_Xab[b]							
08-May-2013	uid___A002_X62932c_X188[a]	6/9	1924-292	26	0.47	29	yes	no
09-May-2013	uid___A002_X62a5df_X33	6/9	3c279	33	0.36	29	yes	no
	uid___A002_X62a5df_X66[b]							

Notes: [a] *This observation had low S/N in both bands and did not give good solutions. I need to look more carefully at these data to figure out why (possibly bad WVR); for now, I do not include this data-set in the analysis.* [b] *This execution was run immediately after the previous one using the same settings, so I concatenate these data for all analyses in this report.*

Table 2: Band 7 Calibrated by Band 3: interp='linear'

ASDM(s)	Phase r.m.s. (deg) Self-cal	Phase r.m.s. (deg) low-ν cal	Fractional Increase in r.m.s.	Mean Phase (deg) low-ν cal
Xc87	10.4 (7.6 - 12.8)	13.1 (8.6 - 17.3)	0.25 (0.04 - 0.51)	2.7 (-4.3 - 11.3)
X12	4.1 (2.8 - 6.1)	8.9 (3.7 - 16.4)	1.15 (0.22 - 2.27)	1.3 (-2.3 - 9.4)
X4a5	4.5 (3.0 - 6.1)	8.6 (4.5 - 13.1)	0.89 (0.33 - 1.60)	1.3 (-2.9 - 8.1)
X530	6.4 (4.0 - 9.9)	14.4 (9.5 - 22.5)	1.25 (0.46 - 2.29)	1.0 (-6.6 - 5.2)
X717	6.0 (4.0 - 8.2)	9.5 (5.9 - 14.5)	0.60 (0.12 - 1.63)	-1.6 (-6.1 - 2.7)
X129	6.1 (4.2 - 19.1)	9.1 (5.6 - 20.1)	0.54 (0.05 - 1.45)	3.8 (-4.3 - 18.0)
X358	1.9 (1.3 - 2.7)	5.5 (2.2 - 10.2)	1.71 (0.38 - 3.16)	0.3 (-3.1 - 5.0)
X2f6+X327	2.9 (1.8 - 14.7)	11.0 (3.4 - 22.7)	4.01 (0.42 - 11.65)	4.6 (-3.1 - 15.6)
X3a+X6b	3.9 (3.2 - 4.8)	13.5 (6.9 - 21.5)	2.39 (1.10 - 4.16)	1.4 (-11.1 - 13.4)

Notes: For each column, the first value is the mean from all antennas, and the range listed in parentheses shows the minimum and maximum values. Column four shows the fractional increase in the corrected phase r.m.s. when using the low-frequency gain solutions to calibrate the high frequency data.

Table 3: Band 7 Calibrated by Band 3: interp='linearPD'

ASDM(s)	Phase r.m.s. (deg) Self-cal	Phase r.m.s. (deg) low-ν cal	Fractional Increase in r.m.s.	Mean Phase (deg) low-ν cal
Xc87	10.4 (7.6 - 12.8)	15.1 (8.8 - 22.6)	0.44 (0.05 - 1.06)	8.0 (-4.5 - 25.9)
X12	4.1 (2.8 - 6.1)	9.5 (4.3 - 16.3)	1.28 (0.41 - 2.25)	1.4 (-3.8 - 7.9)
X4a5	4.5 (3.0 - 6.1)	9.3 (4.8 - 14.0)	1.05 (0.27 - 1.78)	0.2 (-4.4 - 8.1)
X530	6.4 (4.0 - 9.9)	16.6 (9.3 - 23.5)	1.59 (0.51 - 2.58)	-0.2 (-11.9 - 12.3)
X717	6.0 (4.0 - 8.2)	10.7 (6.8 - 16.0)	0.80 (0.22 - 1.75)	-3.5 (-9.0 - 1.3)
X129	6.1 (4.2 - 19.1)	10.3 (6.0 - 22.4)	0.76 (0.15 - 1.77)	6.9 (-3.0 - 32.2)
X358	1.9 (1.3 - 2.7)	6.1 (2.0 - 10.2)	2.01 (0.42 - 5.11)	0.7 (-5.3 - 5.2)
X2f6+X327	2.9 (1.8 - 14.7)	8.7 (3.5 - 20.0)	2.77 (0.37 - 4.77)	-0.3 (-4.5 - 5.1)
X3a+X6b	3.9 (3.2 - 4.8)	15.1 (10.6 - 22.6)	2.85 (1.82 - 4.66)	-14.2 (-22.6 - -6.5)

Notes: For each column, the first value is the mean from all antennas, and the range listed in parentheses shows the minimum and maximum values. Column four shows the fractional increase in the corrected phase r.m.s. when using the low-frequency gain solutions to calibrate the high frequency data.

Table 4: Band 9 Calibrated by Band 6: interp='linear'

ASDM(s)	Phase r.m.s. (deg) Self-cal	Phase r.m.s. (deg) low-ν cal	Fractional Increase in r.m.s.	Mean Phase (deg) low-ν cal
X1c5+X202	19.0 (15.0 - 27.0)	16.1 (10.3 - 26.4)	-0.13 (-0.36 - 0.23)	0.1 (-5.4 - 4.8)
X6e+Xab	24.1 (19.5 - 37.2)	25.7 (15.0 - 52.2)	0.07 (-0.23 - 1.36)	-1.1 (-21.5 - 18.2)
X33+X66	9.2 (3.0 - 19.2)	25.9 (10.2 - 54.1)	2.90 (-0.14 - 8.95)	-0.9 (-17.7 - 17.9)

Notes: For each column, the first value is the mean from all antennas, and the range listed in parentheses shows the minimum and maximum values. Column four shows the fractional increase in the corrected phase r.m.s. when using the low-frequency gain solutions to calibrate the high frequency data.

Table 5: Band 9 Calibrated by Band 6: interp='linearPD'

ASDM(s)	Phase r.m.s. (deg) Self-cal	Phase r.m.s. (deg) low-ν cal	Fractional Increase in r.m.s.	Mean Phase (deg) low-ν cal
X1c5+X202	19.0 (15.0 - 27.0)	20.0 (10.9 - 31.2)	0.08 (-0.32 - 0.99)	-1.8 (-7.4 - 5.4)
X6e+Xab	24.1 (19.5 - 37.2)	28.4 (16.0 - 55.6)	0.18 (-0.18 - 1.51)	-1.9 (-25.9 - 15.9)
X33+X66	9.2 (3.0 - 19.2)	27.1 (11.2 - 53.8)	3.09 (-0.34 - 8.88)	-6.3 (-30.9 - 11.7)

Notes: For each column, the first value is the mean from all antennas, and the range listed in parentheses shows the minimum and maximum values. Column four shows the fractional increase in the corrected phase r.m.s. when using the low-frequency gain solutions to calibrate the high frequency data.

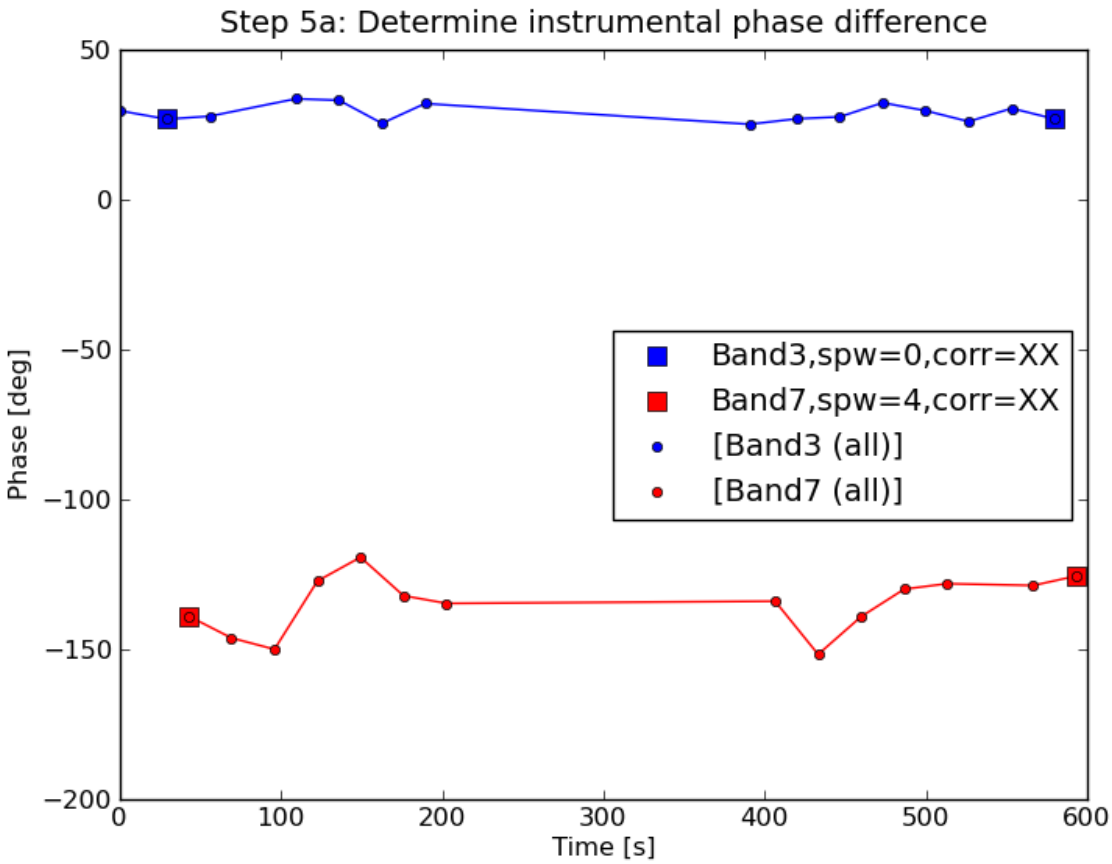

Figure 1: Demonstrates Step 5a of the BBPT data processing described in Section 4, where the instrumental phase difference between the low and high frequency bands are determined. This is from a single observation (X3a+X6b), switching between Band 3 (blue) and Band 7 (red) on 3c279, and shows only two spws and the XX polarization for one antenna. The small circles show the results from running **gaincal** on all scans; the resulting table is *not* used for futher calibration, but is shown only to demonstrate the phase variations over the course of the observation and the scan sequence. The large squares show the beginning and end scan pairs used to derive the instrumental phase difference between the two bands. The gain table derived from these scan pairs is applied to the Band 3 and Band 7 data in Steps 5b and 5c.

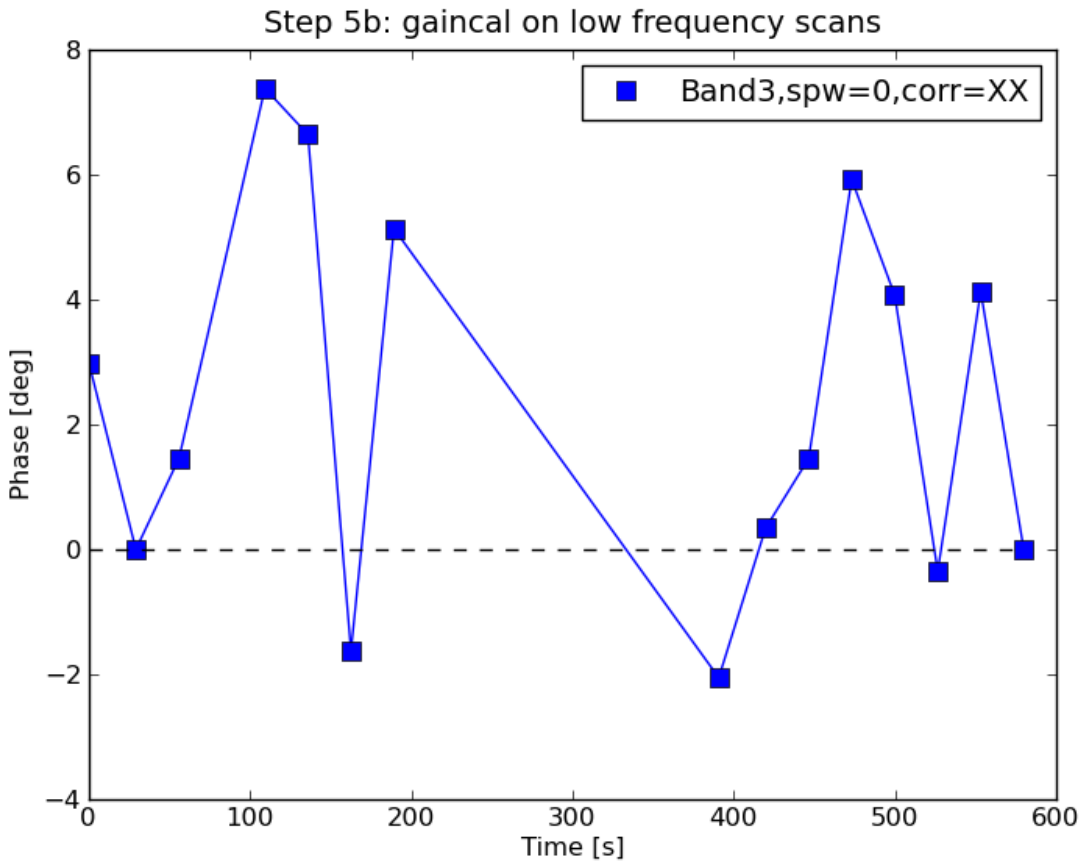

Figure 2: Demonstrates Step 5b of the BBPT data processing described in Section 4, where the phase solution is determined from the low frequency data *after* applying the instrumental phase offset determined in Step 5a (note that the scans used to derive this offset are now at 0° as expected). This gain table is applied to the Band 7 data in Step 5c. See caption to Figure 1 for details of this observation.

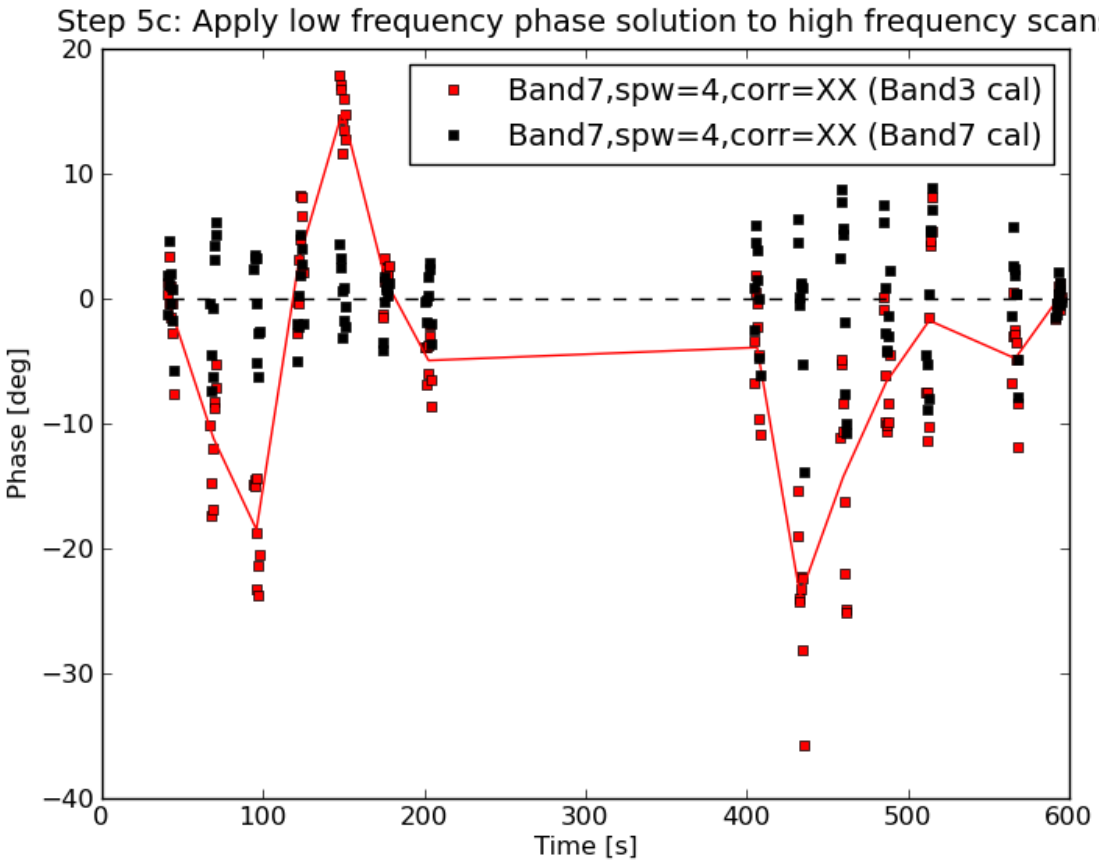

Figure 3: Demonstrates Step 5c of the BBPT data processing described in Section 4, where the phase solution from the low frequency data is applied to the high frequency data. The red squares show the corrected Band 7 phases calibrated by Band 3 (per integration, averaged over all channels), and the red curve traces the per-scan average. In this case I used interp='linear' (does not scale the phases by the frequency ratio). The black squares show the results using Band 7 to calibrate Band 7 for comparison. See caption to Figure 1 for details of this observation.

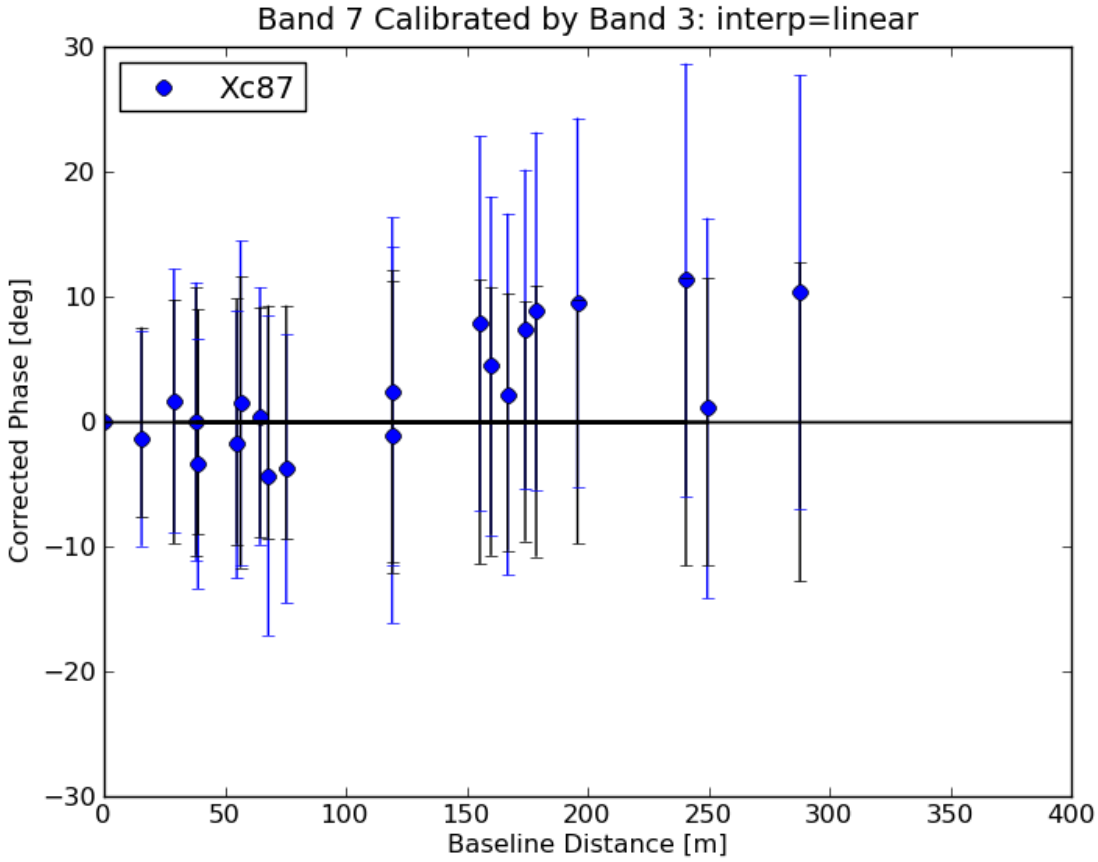

Figure 4: Mean corrected phase for each antenna as a function of baseline distance for the observation Xc87. The Band 7 data were calibrated using the Band 3 gain solutions with interp='linear' (no scaling of the solutions by the frequency ratio). The blue circles show the mean phase offset averaged over all scans, and the blue error bars show the standard deviation. The black error bars centered on zero show the standard deviation of the corrected phases using Band 7 gain solutions (self-cal). Figures 5 to 12 show the same thing for the other Band 3/Band 7 observations.

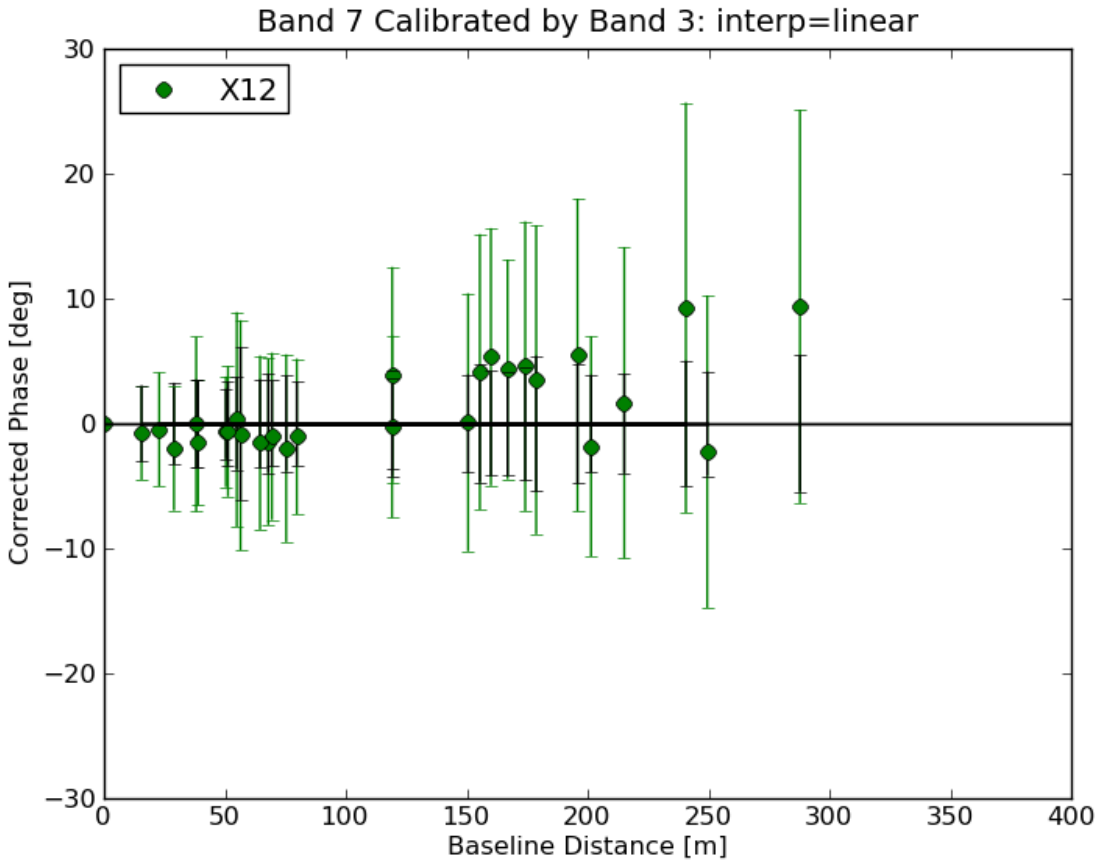

Figure 5: Mean corrected phase for each antenna as a function of baseline distance for the observation X12. See the caption to Figure 4 for a full description.

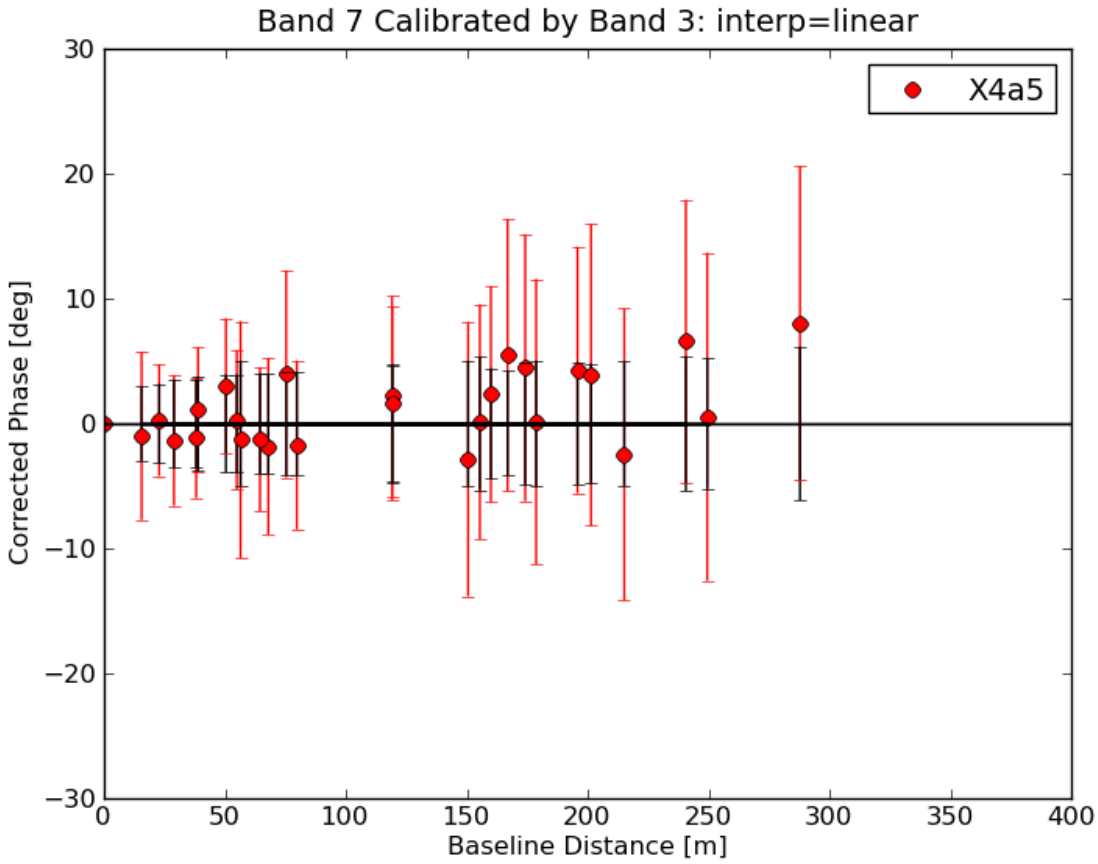

Figure 6: Mean corrected phase for each antenna as a function of baseline distance for the observation X4a5. See the caption to Figure 4 for a full description.

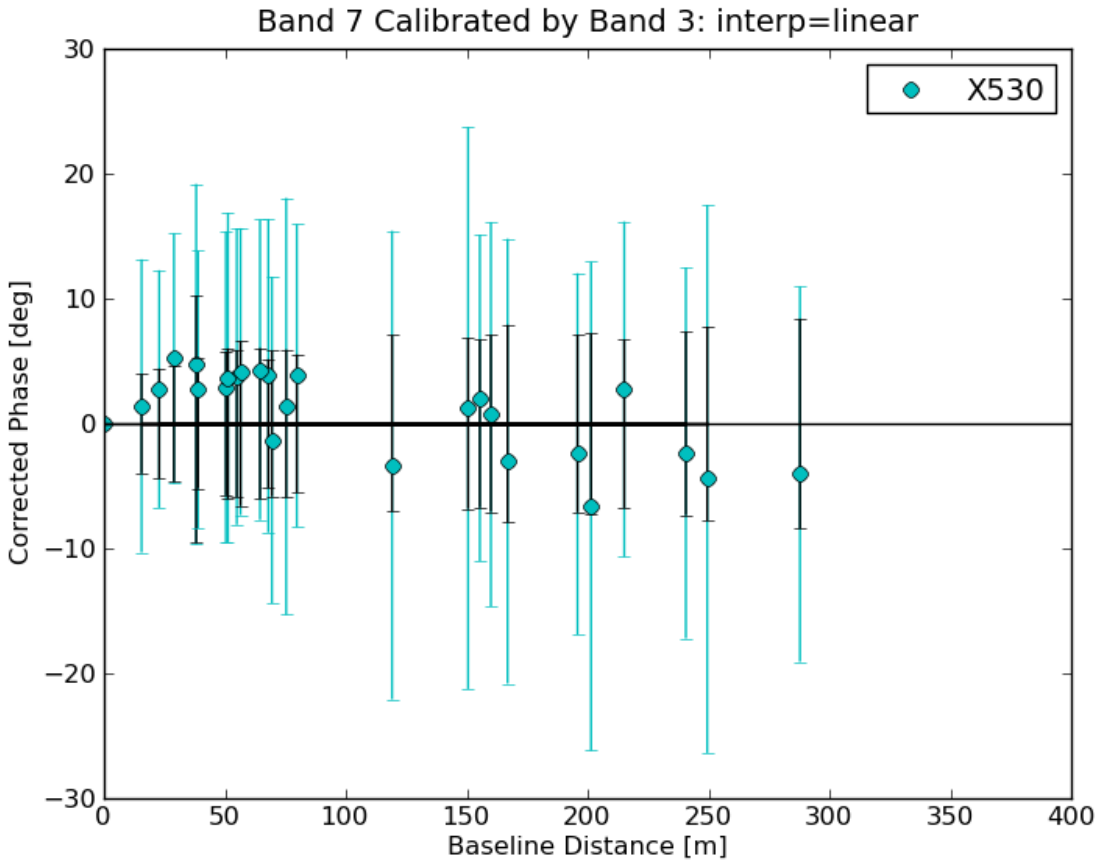

Figure 7: Mean corrected phase for each antenna as a function of baseline distance for the observation X530. See the caption to Figure 4 for a full description.

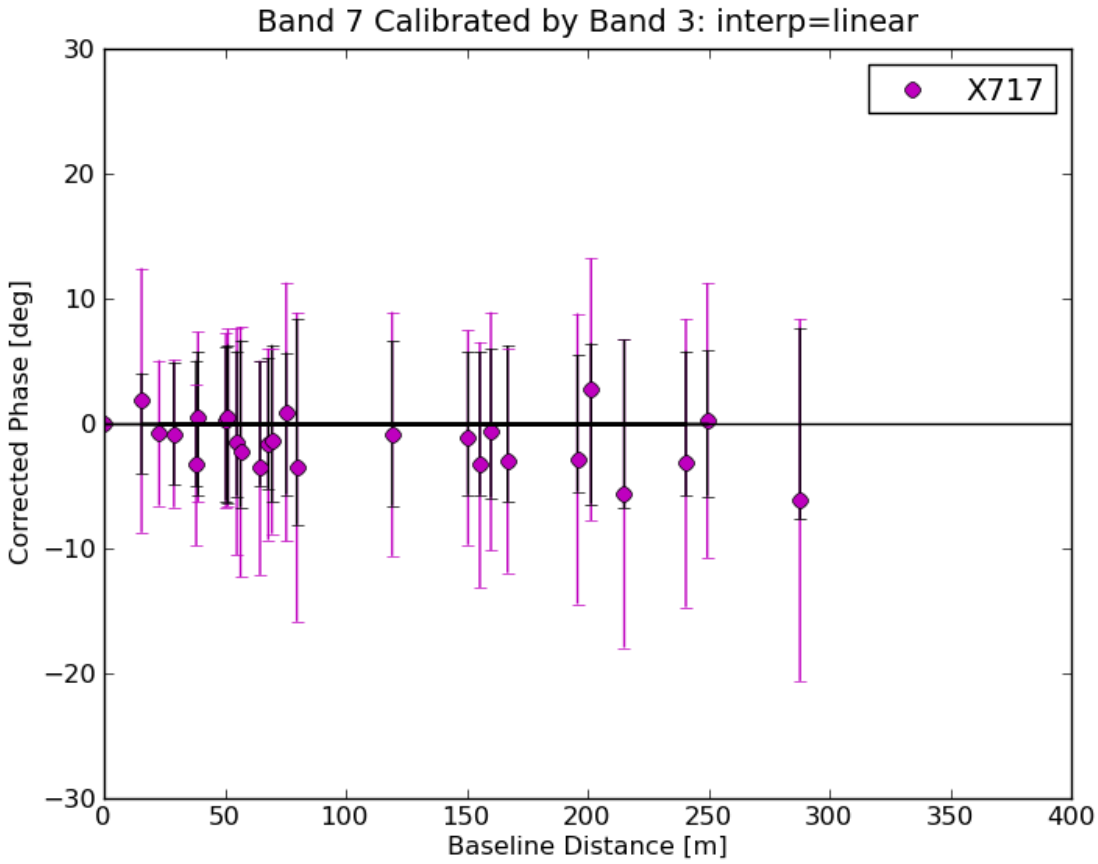

Figure 8: Mean corrected phase for each antenna as a function of baseline distance for the observation X717. See the caption to Figure 4 for a full description.

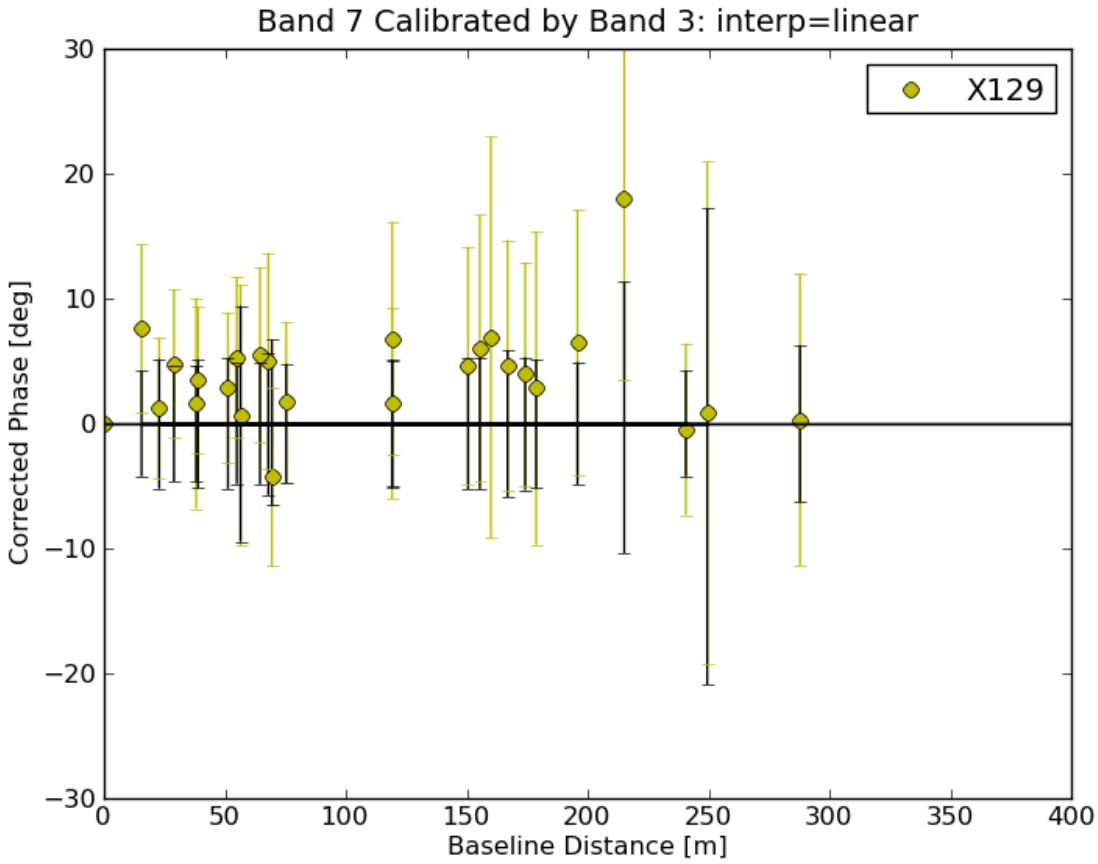

Figure 9: Mean corrected phase for each antenna as a function of baseline distance for the observation X129. See the caption to Figure 4 for a full description.

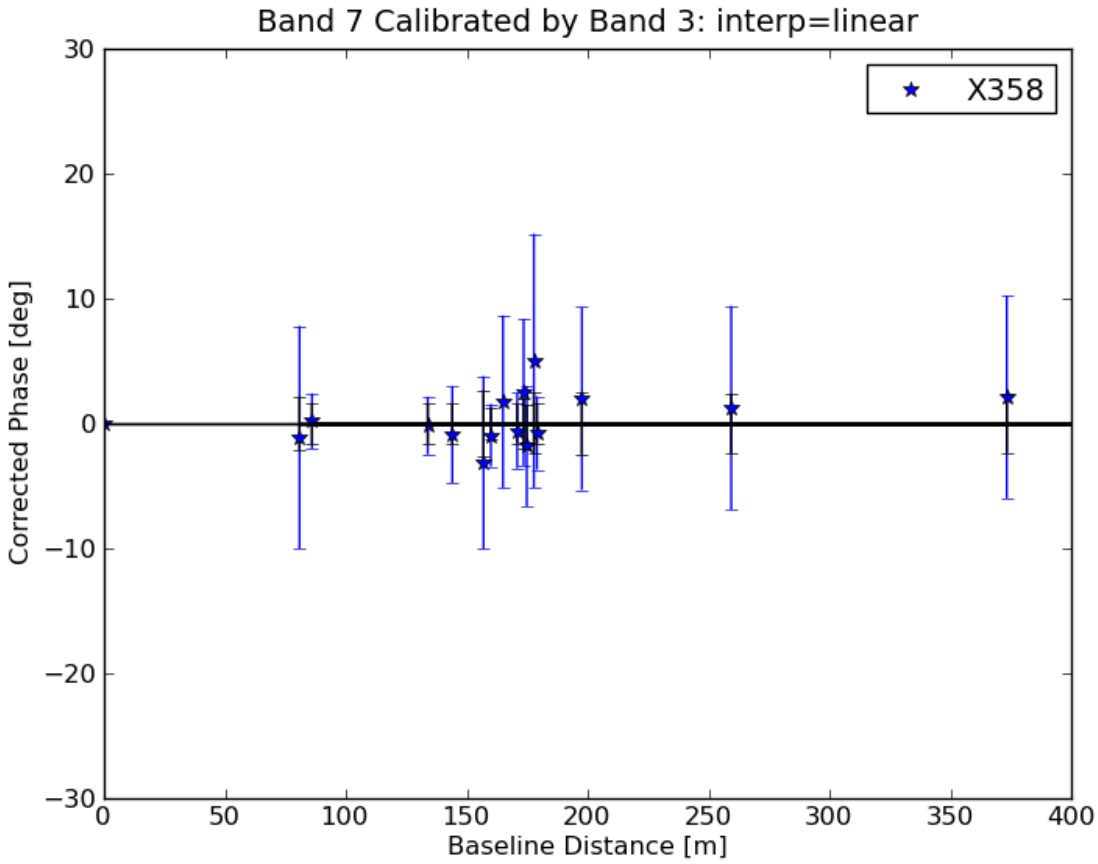

Figure 10: Mean corrected phase for each antenna as a function of baseline distance for the observation X358. See the caption to Figure 4 for a full description.

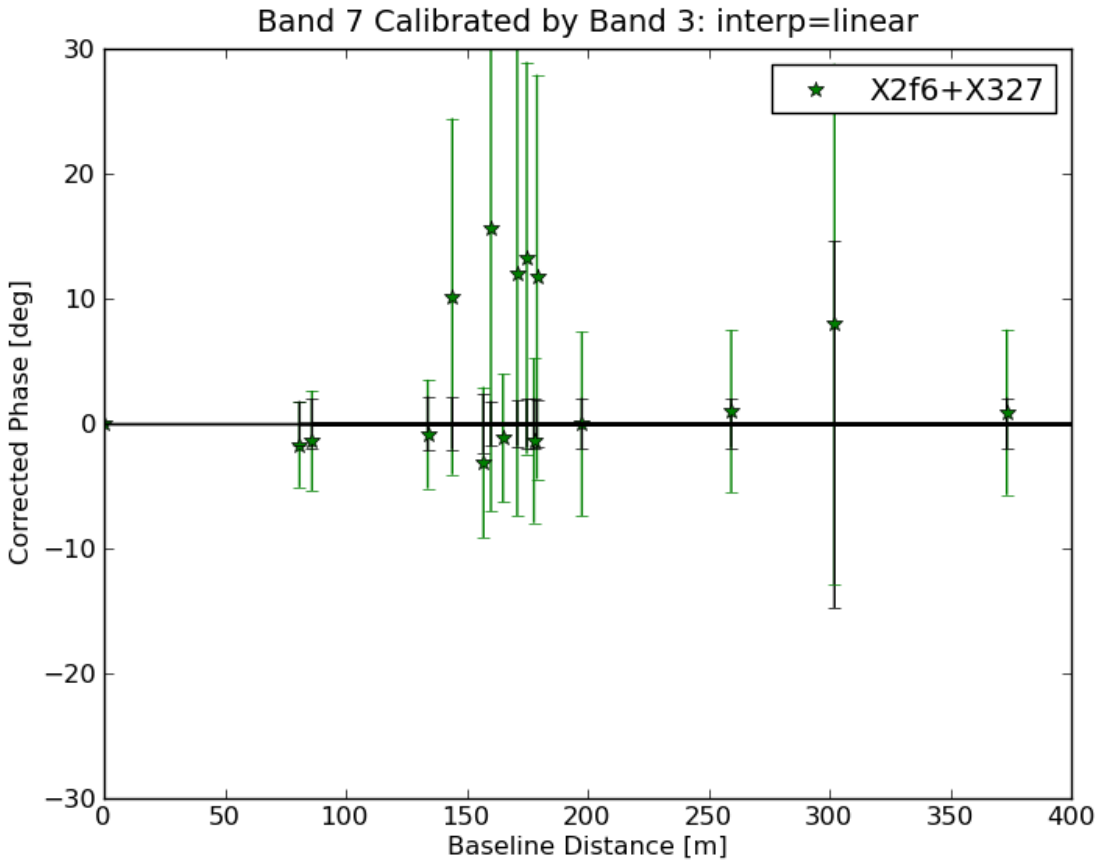

Figure 11: Mean corrected phase for each antenna as a function of baseline distance for the observation X2f6+X327. See the caption to Figure 4 for a full description.

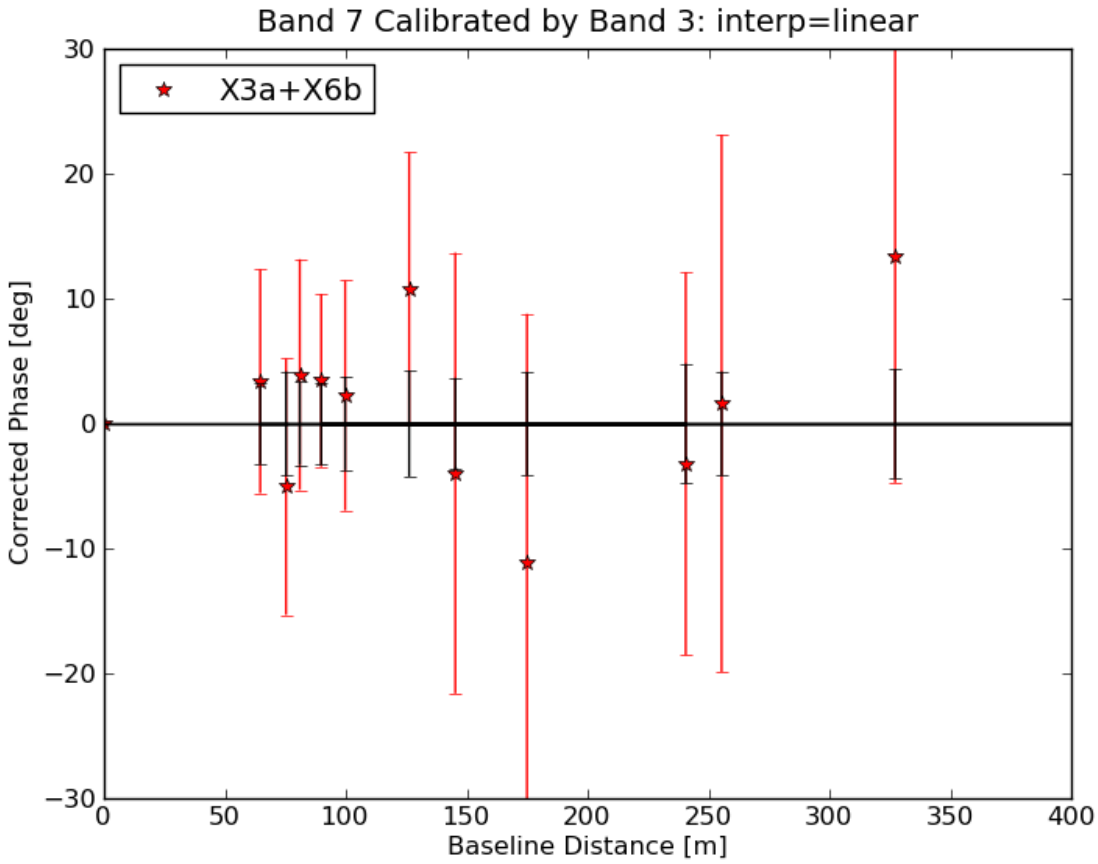

Figure 12: Mean corrected phase for each antenna as a function of baseline distance for the observation X3a+X6b. See the caption to Figure 4 for a full description.

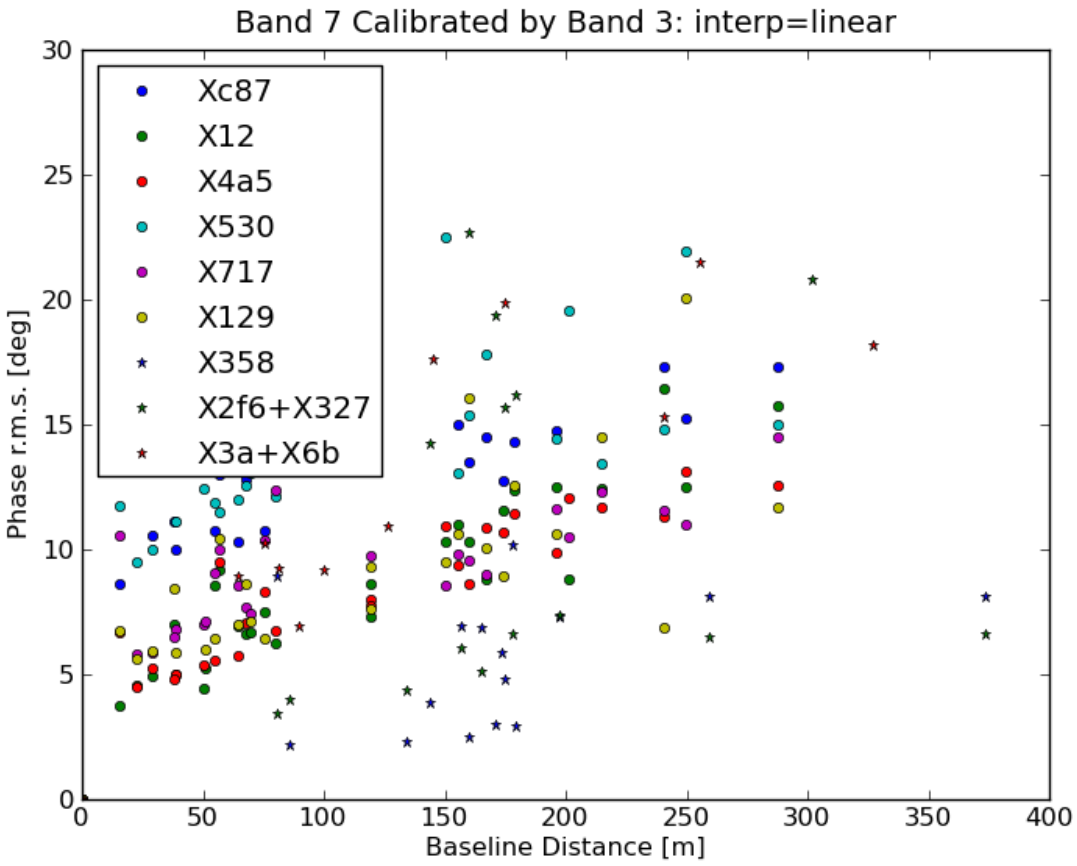

Figure 13: Corrected phase r.m.s. for each antenna as a function of baseline distance for all Band 3/Band 7 observations as labeled, using interp='linear' (no scaling of the solutions by the frequency ratio).

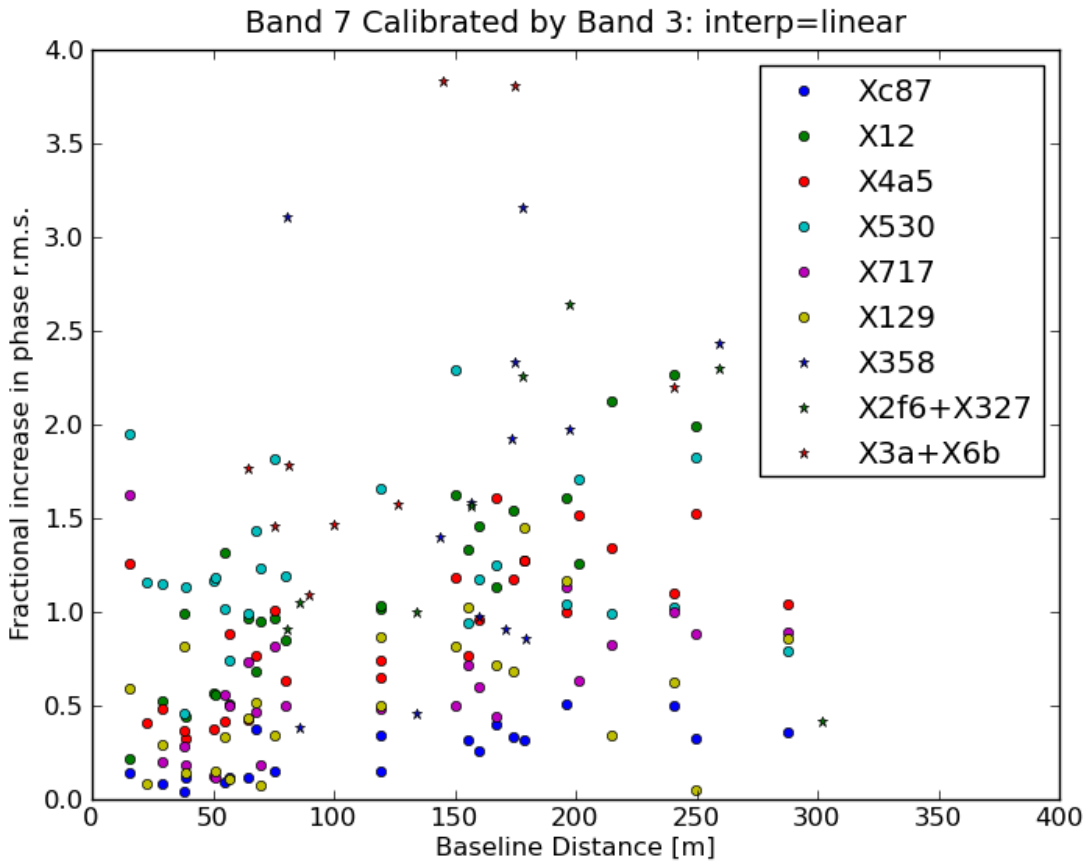

Figure 14: Fractional increase in the corrected phase r.m.s. for each antenna as a function of baseline distance for all Band 3/Band 7 observations as labeled, using interp='linear' (no scaling of the solutions by the frequency ratio).

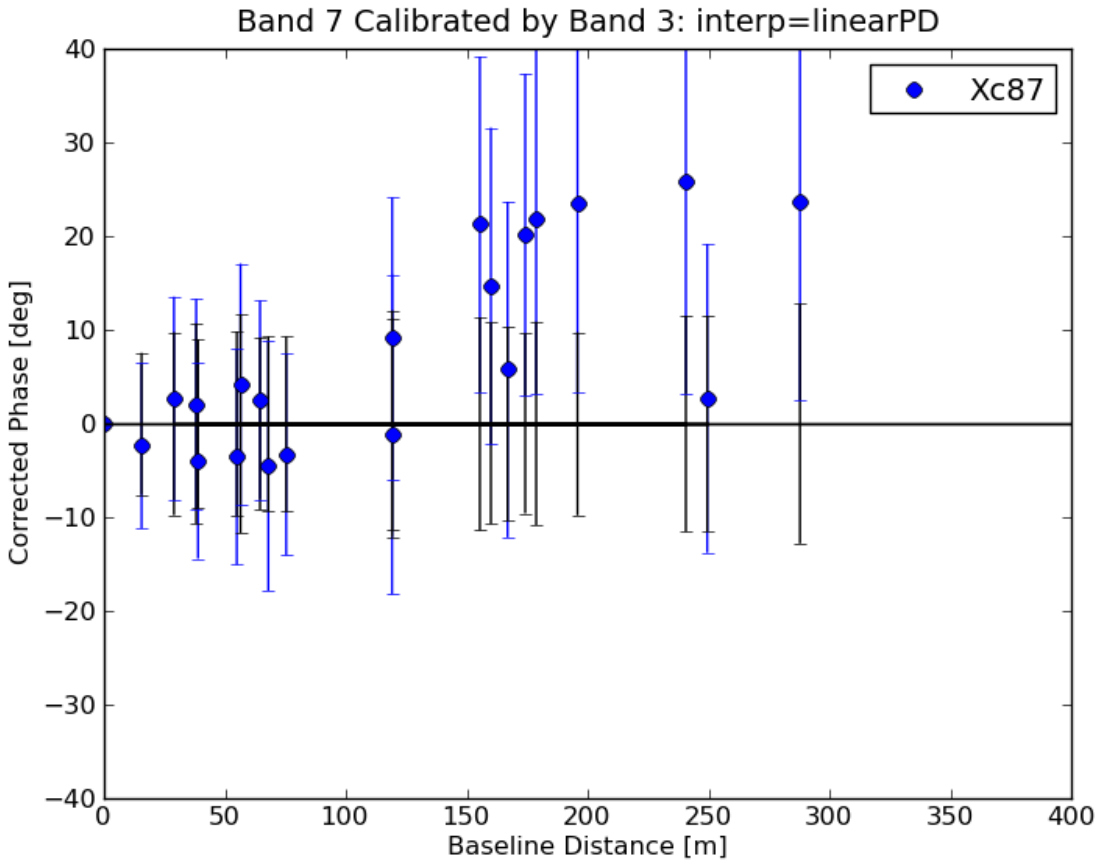

Figure 15: Mean corrected phase for each antenna as a function of baseline distance for the observation Xc87. The Band 7 data were calibrated using the Band 3 gain solutions with interp='linearPD' (scaling of the solutions by the frequency ratio). The blue circles show the mean phase offset averaged over all scans, and the blue error bars show the standard deviation. The black error bars centered on zero show the standard deviation of the corrected phases using Band 7 gain solutions (self-cal). Figures 16 to 23 show the same thing for the other Band 3/Band 7 observations.

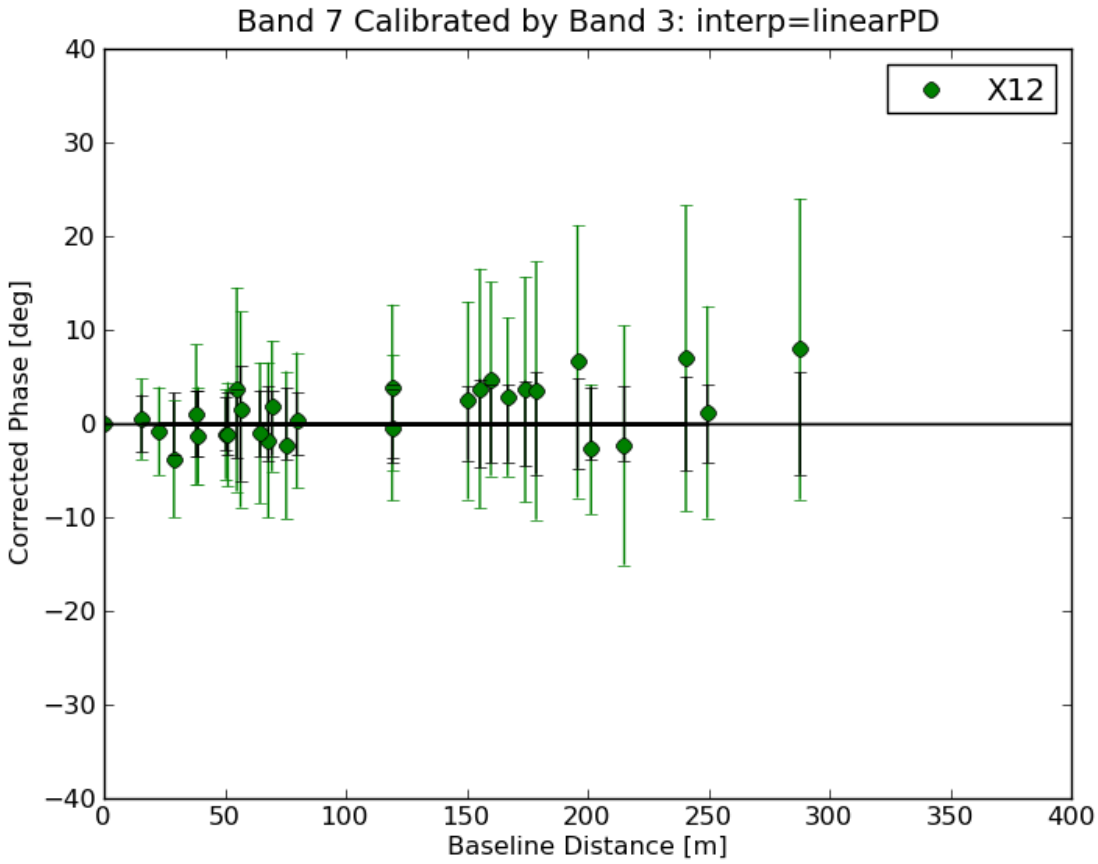

Figure 16: Mean corrected phase for each antenna as a function of baseline distance for the observation X12. See the caption to Figure 15 for a full description.

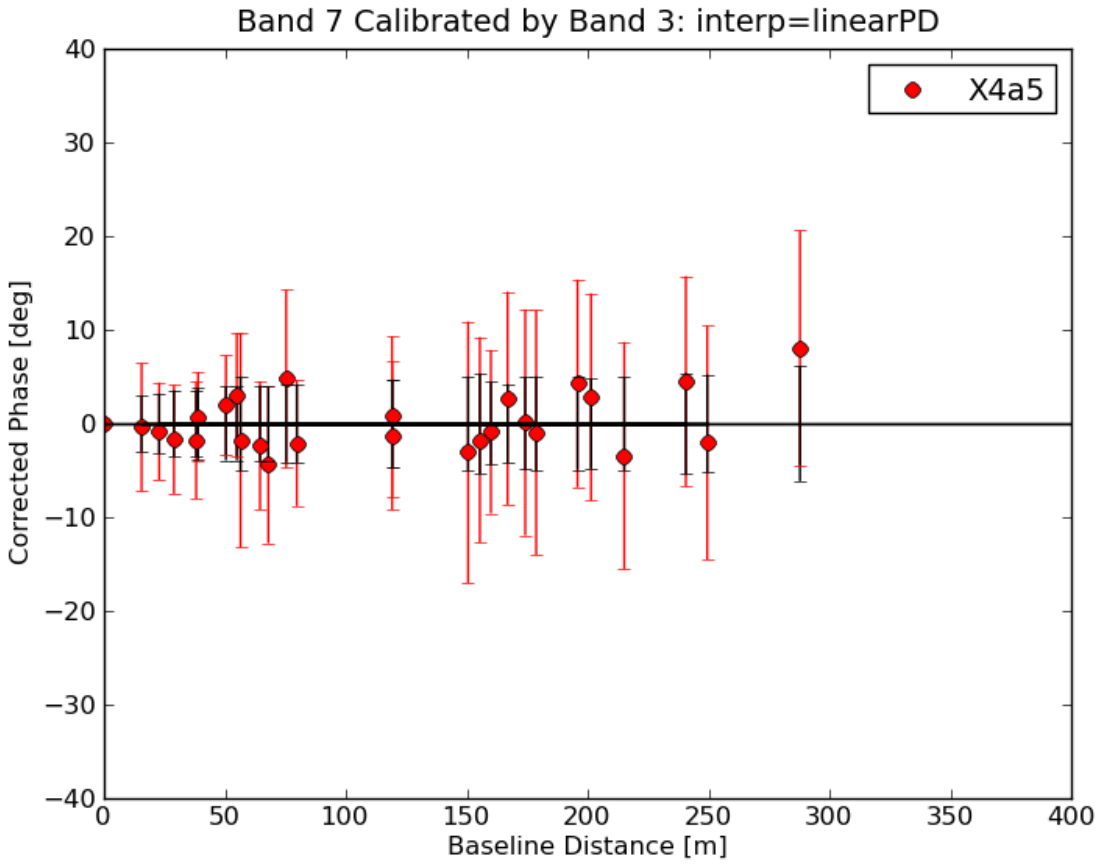

Figure 17: Mean corrected phase for each antenna as a function of baseline distance for the observation X4a5. See the caption to Figure 15 for a full description.

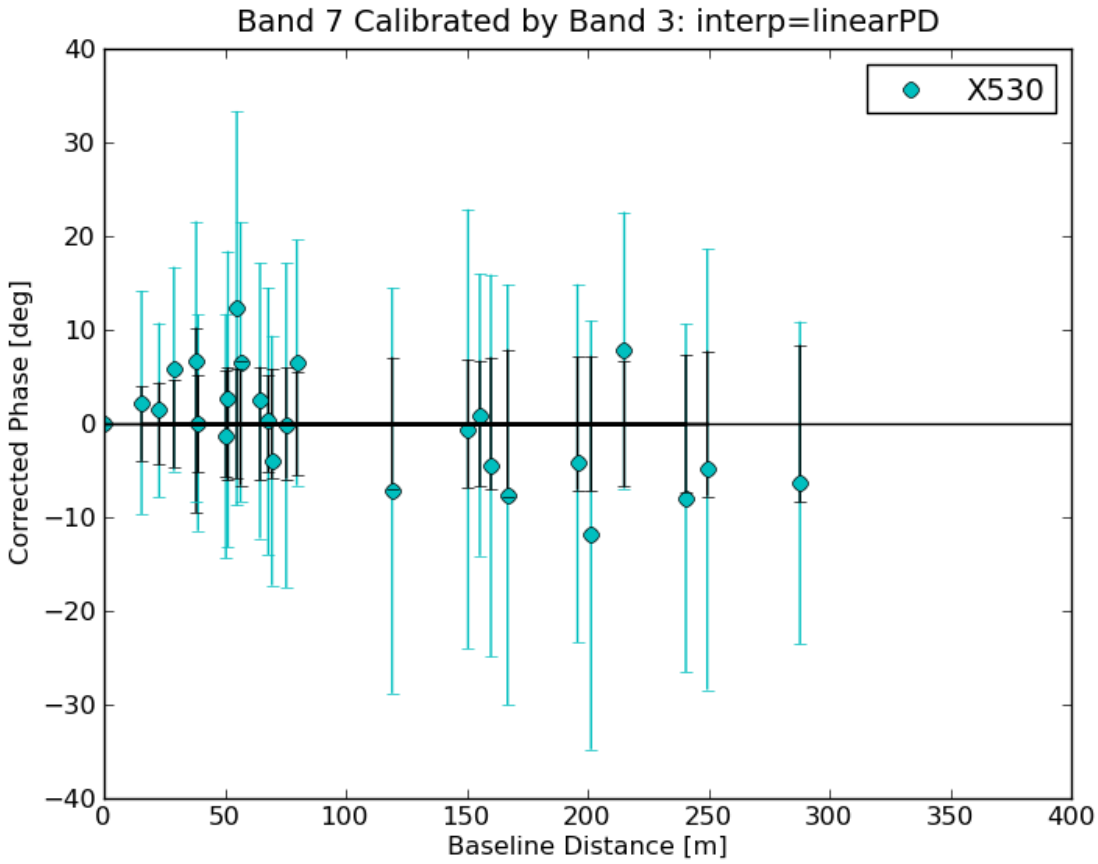

Figure 18: Mean corrected phase for each antenna as a function of baseline distance for the observation X530. See the caption to Figure 15 for a full description.

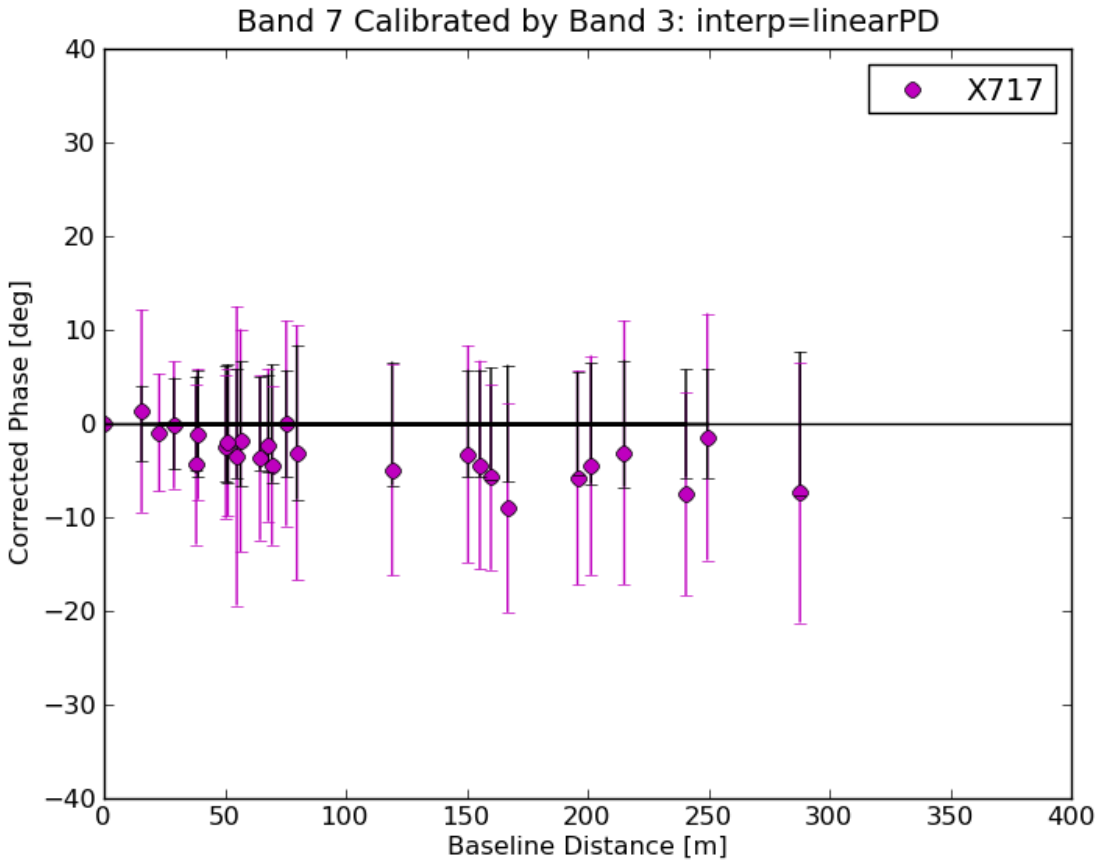

Figure 19: Mean corrected phase for each antenna as a function of baseline distance for the observation X717. See the caption to Figure 15 for a full description.

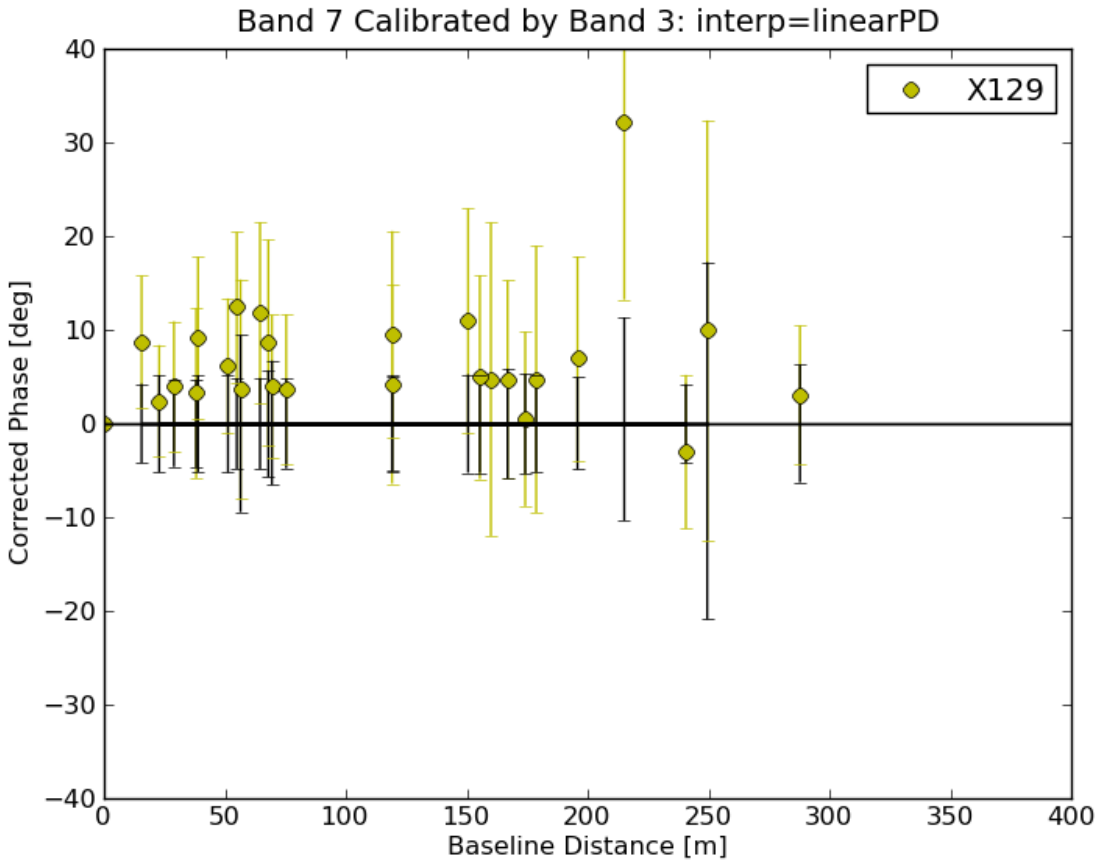

Figure 20: Mean corrected phase for each antenna as a function of baseline distance for the observation X129. See the caption to Figure 15 for a full description.

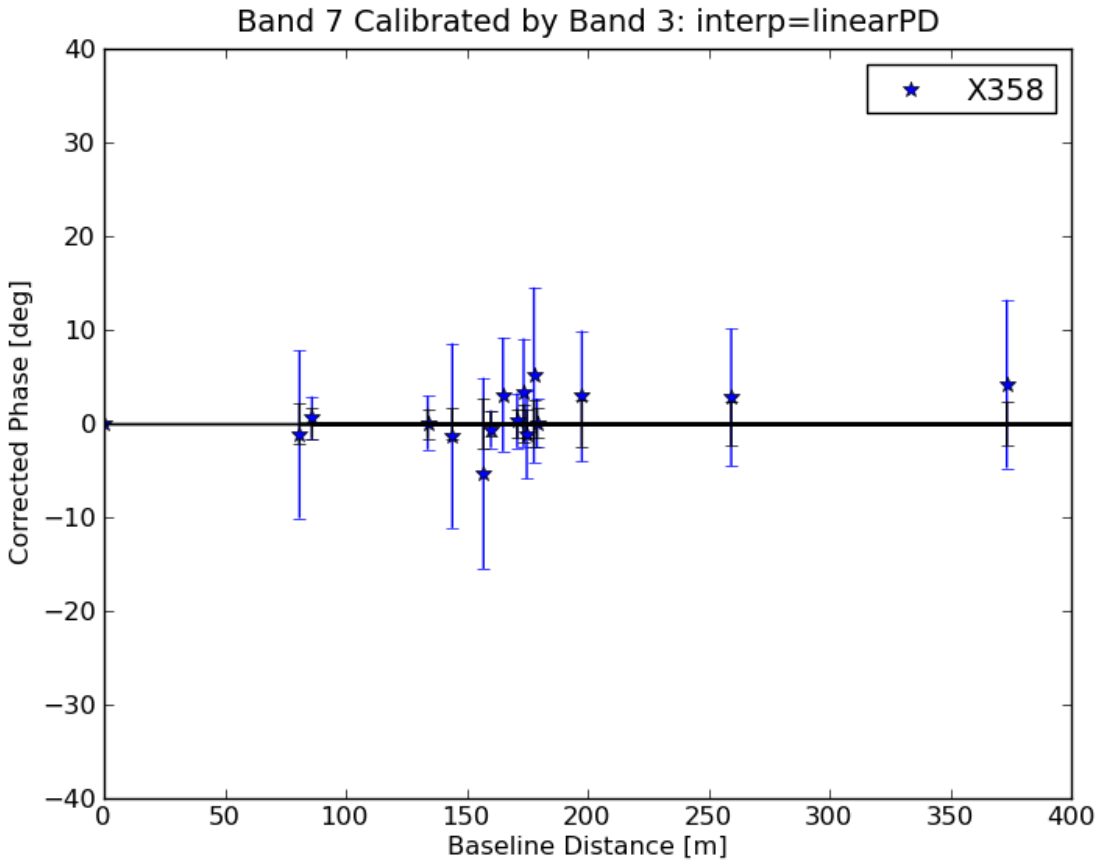

Figure 21: Mean corrected phase for each antenna as a function of baseline distance for the observation X358. See the caption to Figure 15 for a full description.

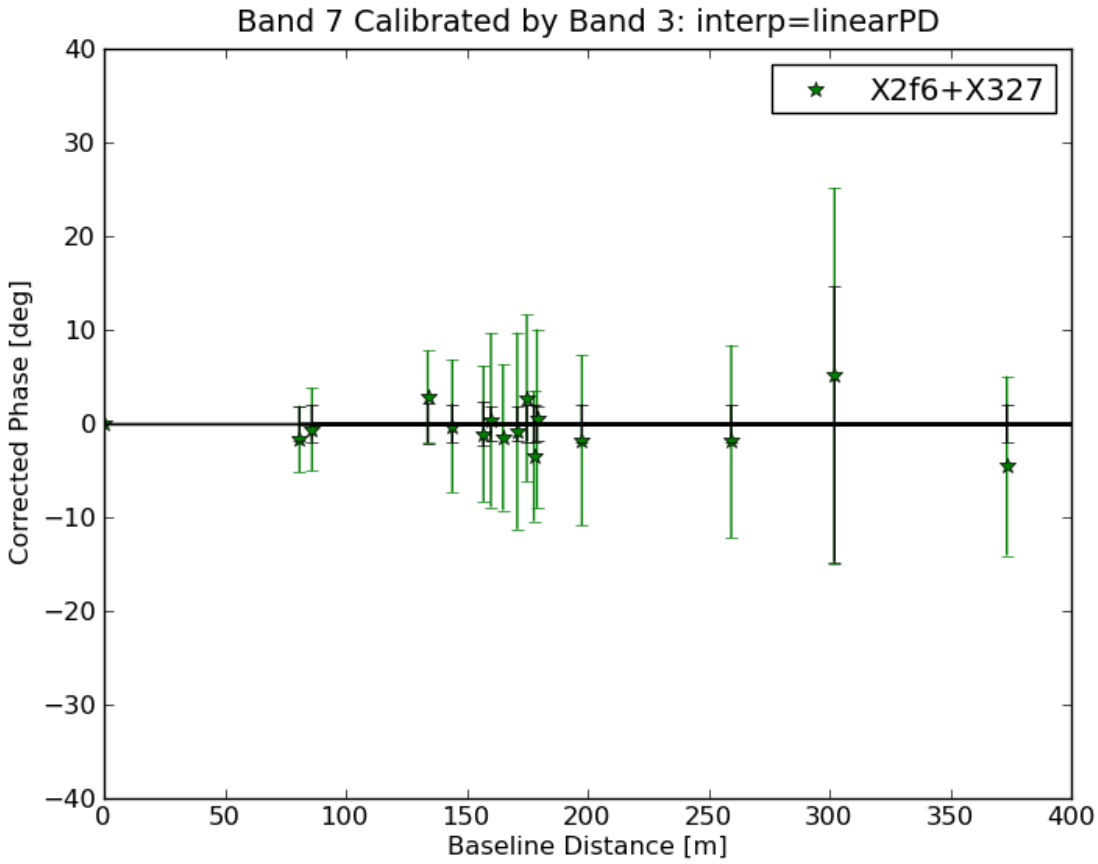

Figure 22: Mean corrected phase for each antenna as a function of baseline distance for the observation X2f6+327. See the caption to Figure 15 for a full description.

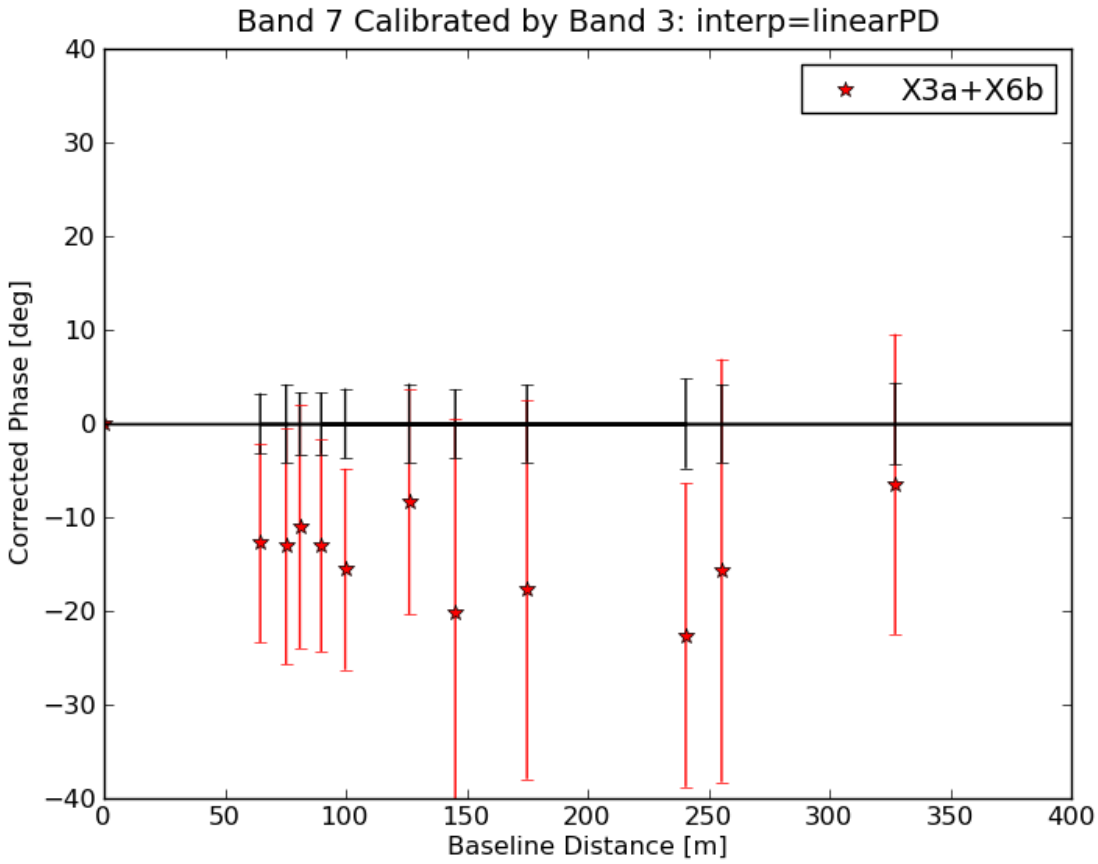

Figure 23: Mean corrected phase for each antenna as a function of baseline distance for the observation X3a+X6b. See the caption to Figure 15 for a full description.

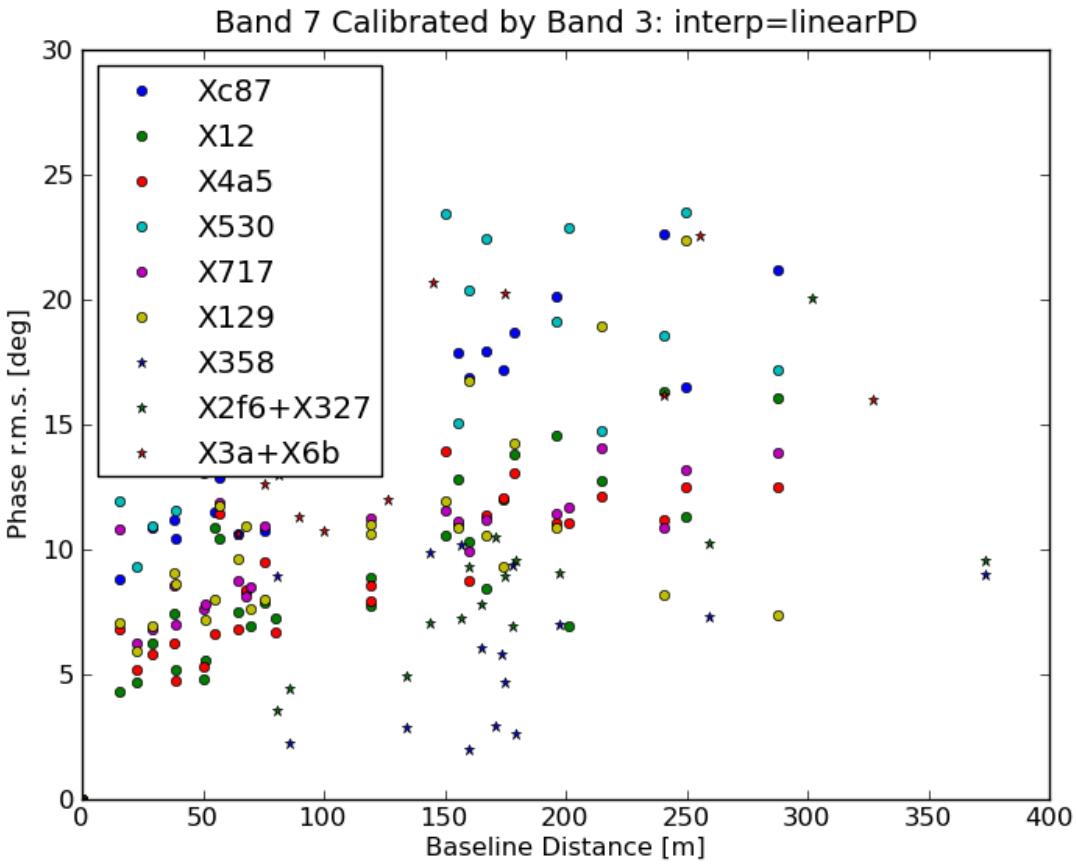

Figure 24: Corrected phase r.m.s. for each antenna as a function of baseline distance for all Band 3/Band 7 observations as labeled, using interp='linearPD' (scaling of the solutions by the frequency ratio).

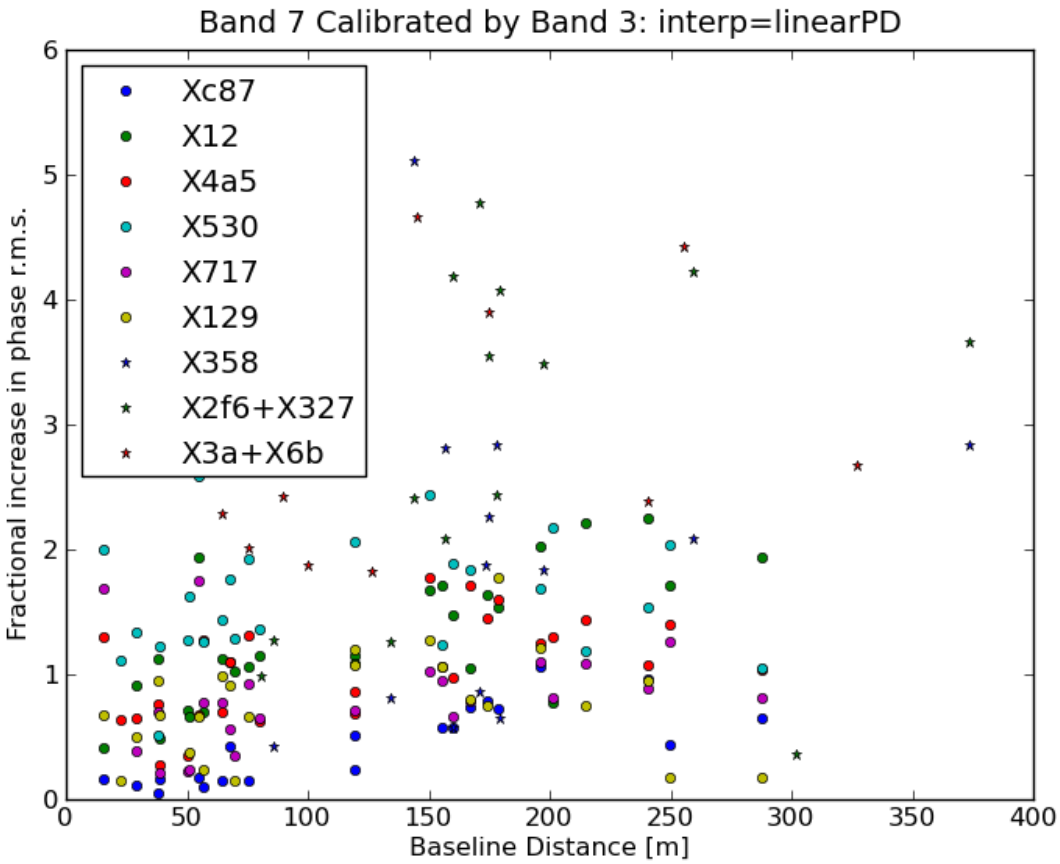

Figure 25: Fractional increase in the corrected phase r.m.s. for each antenna as a function of baseline distance for all Band 3/Band 7 observations as labeled, using interp='linearPD' (scaling of the solutions by the frequency ratio).

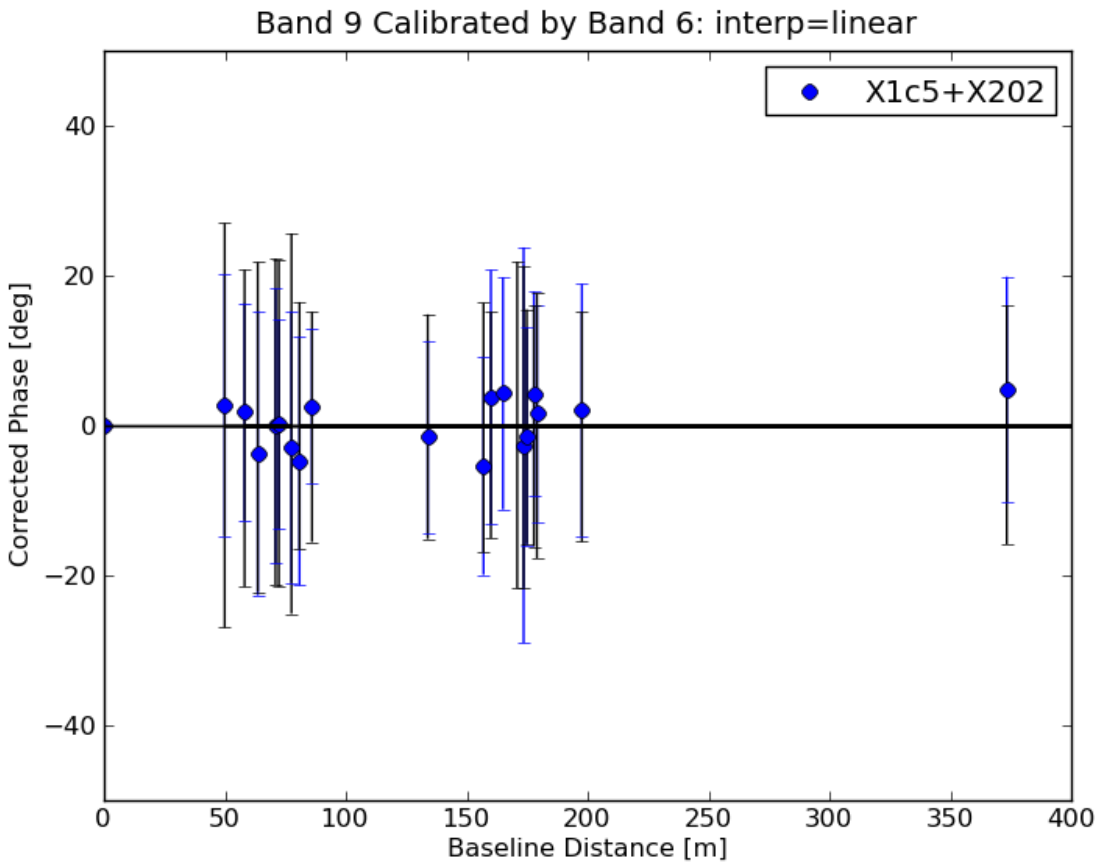

Figure 26: Mean corrected phase for each antenna as a function of baseline distance for the observation X1c5+X202. The Band 9 data were calibrated using the Band 6 gain solutions with interp='linear' (no scaling of the solutions by the frequency ratio). The blue circles show the mean phase offset averaged over all scans, and the blue error bars show the standard deviation. The black error bars centered on zero show the standard deviation of the corrected phases using Band 9 gain solutions (self-cal). Figures 27 to 28 show the same thing for the other Band 6/Band 9 observations.

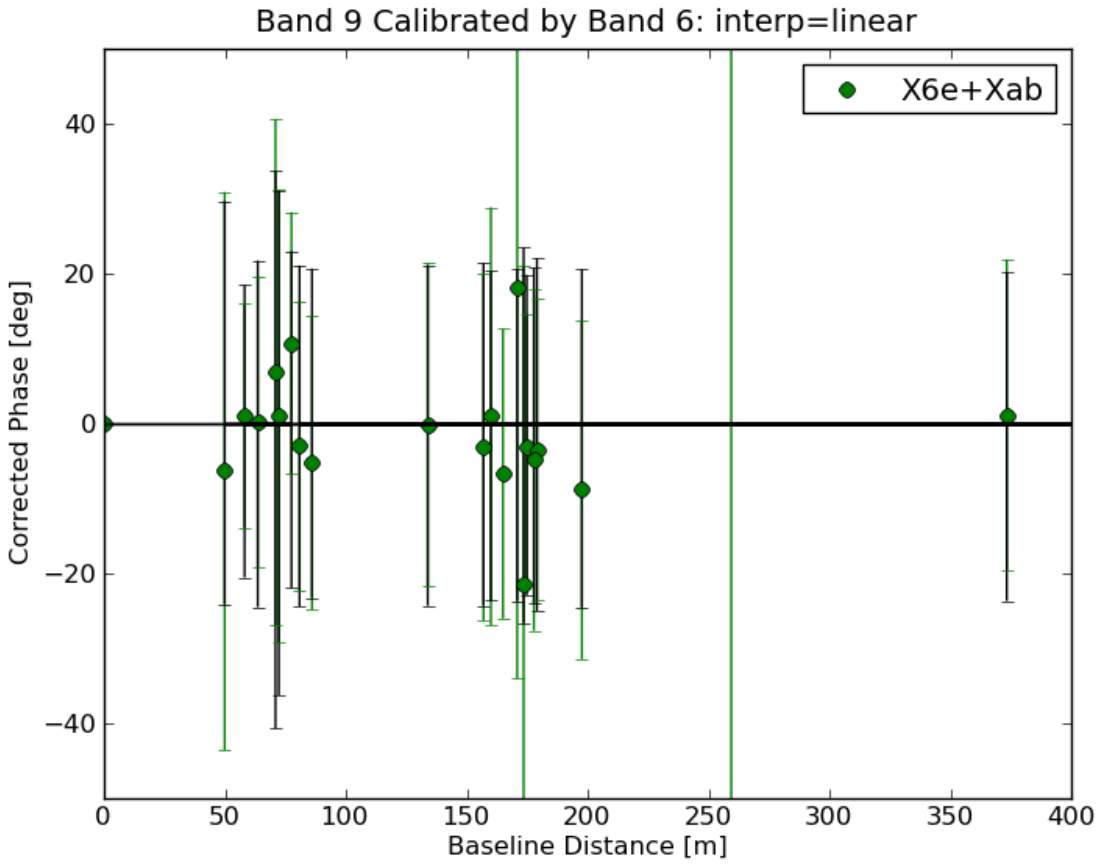

Figure 27: Mean corrected phase for each antenna as a function of baseline distance for the observation X6e+Xab. See the caption to Figure 26 for a full description.

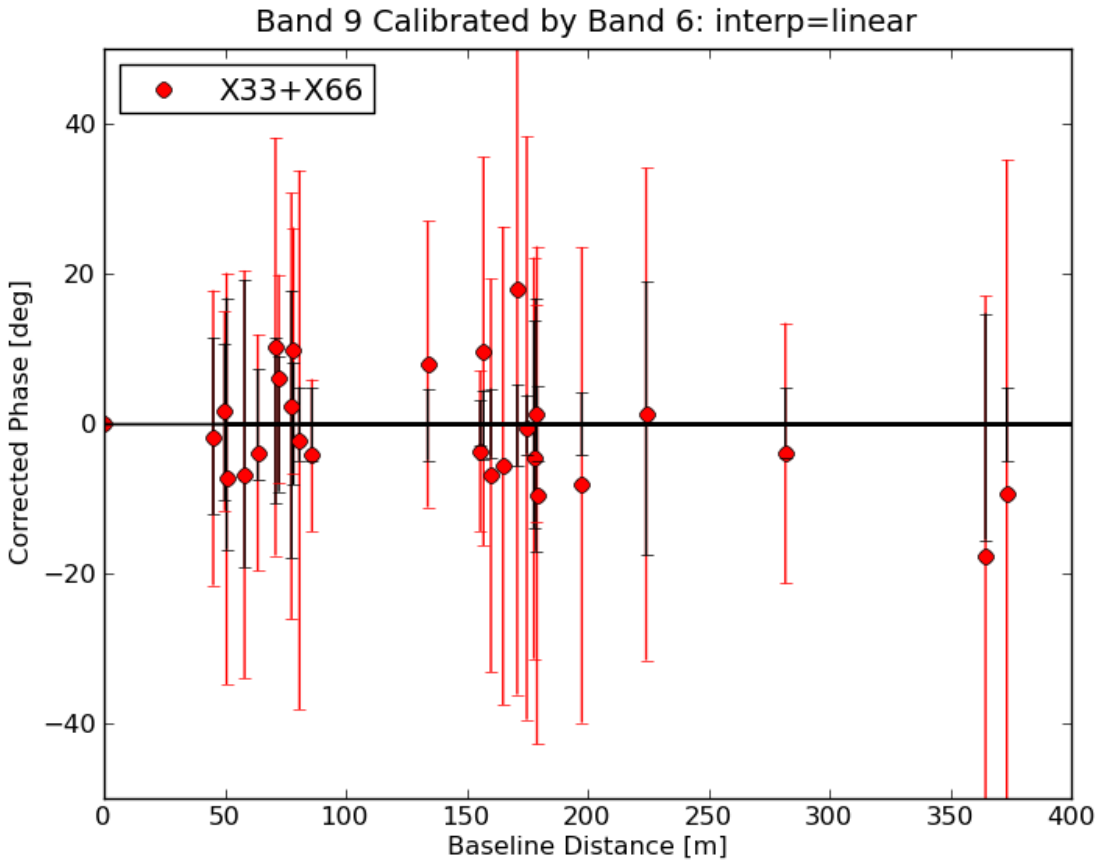

Figure 28: Mean corrected phase for each antenna as a function of baseline distance for the observation X33+X66. See the caption to Figure 26 for a full description.

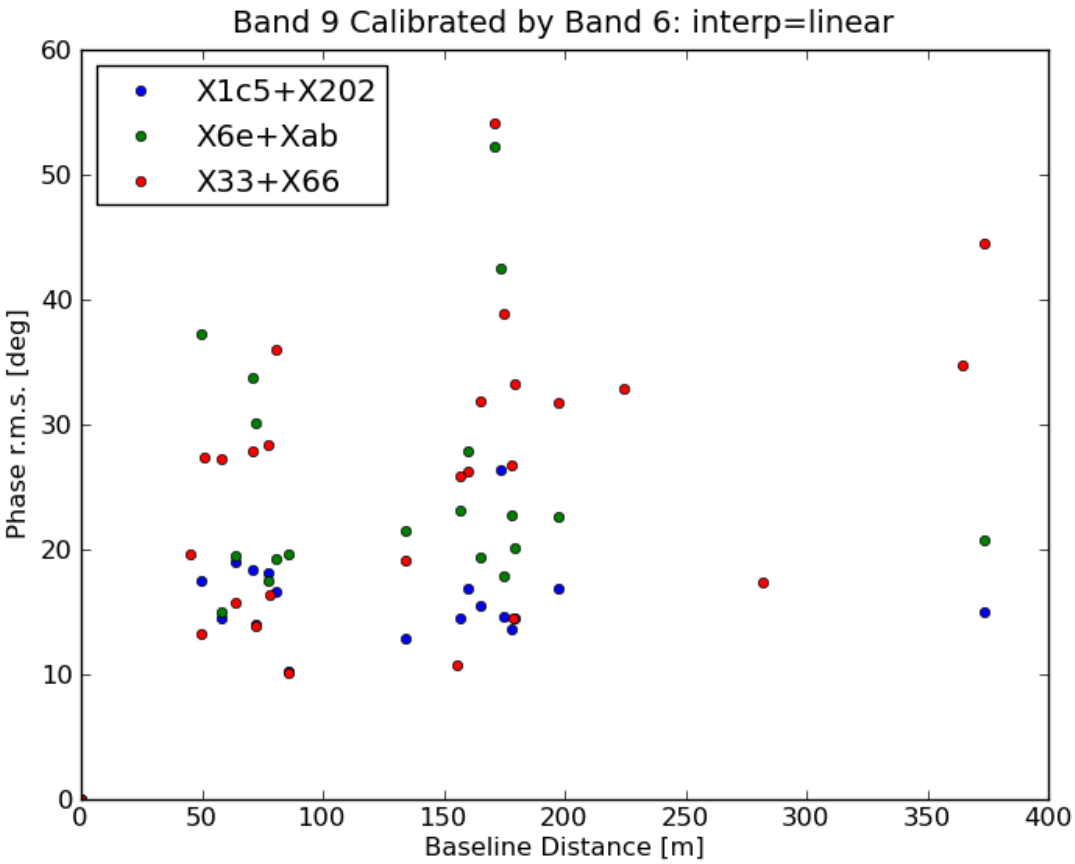

Figure 29: Corrected phase r.m.s. for each antenna as a function of baseline distance for all Band 6/Band 9 observations as labeled, using interp='linear' (no scaling of the solutions by the frequency ratio).

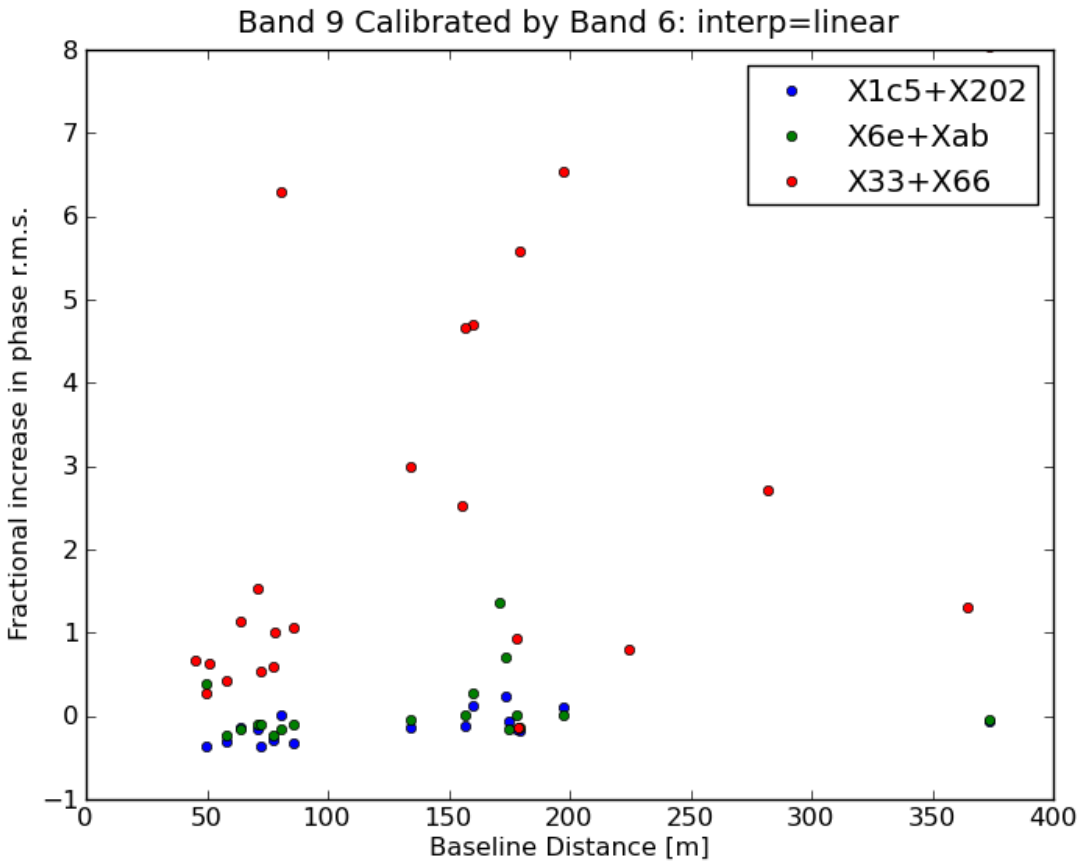

Figure 30: Fractional increase in the corrected phase r.m.s. for each antenna as a function of baseline distance for all Band 6/Band 9 observations as labeled, using interp='linear' (no scaling of the solutions by the frequency ratio).

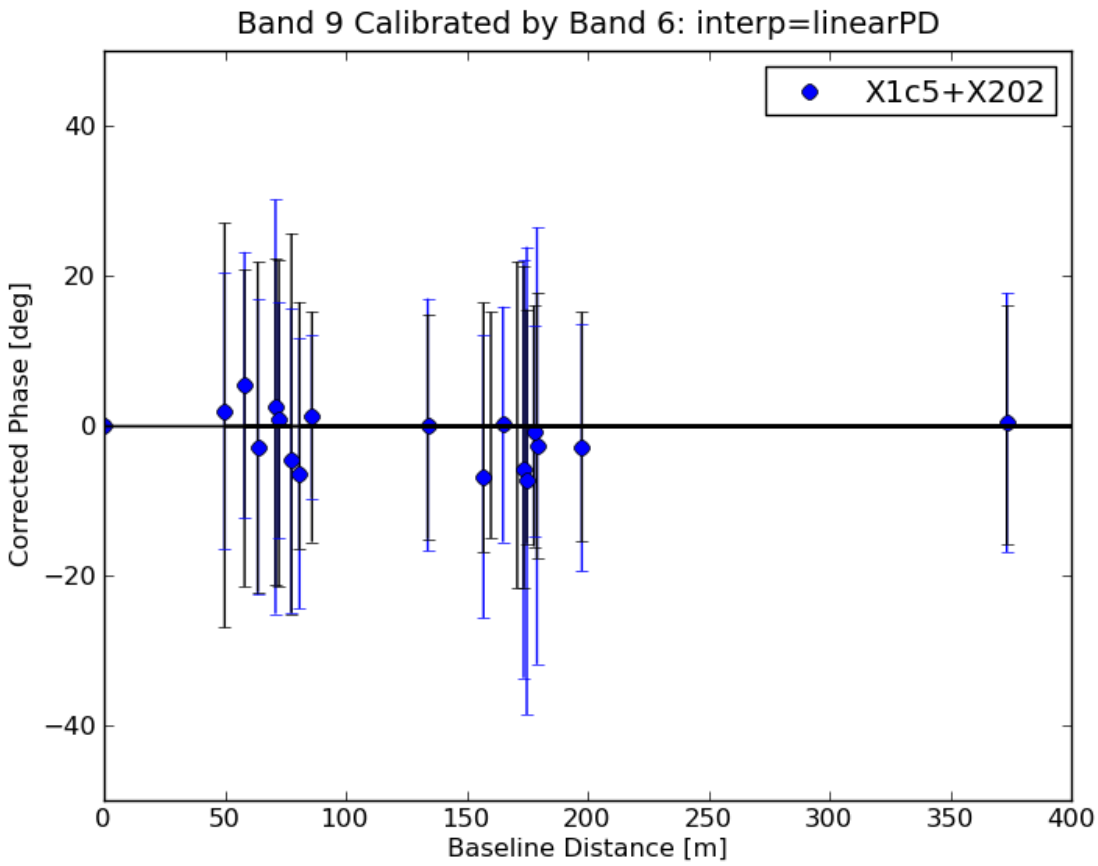

Figure 31: Mean corrected phase for each antenna as a function of baseline distance for the observation X1c5+X202. The Band 9 data were calibrated using the Band 6 gain solutions with interp='linearPD' (scaling of the solutions by the frequency ratio). The blue circles show the mean phase offset averaged over all scans, and the blue error bars show the standard deviation. The black error bars centered on zero show the standard deviation of the corrected phases using Band 9 gain solutions (self-cal). Figures 32 to 33 show the same thing for the other Band6/Band9 observations.

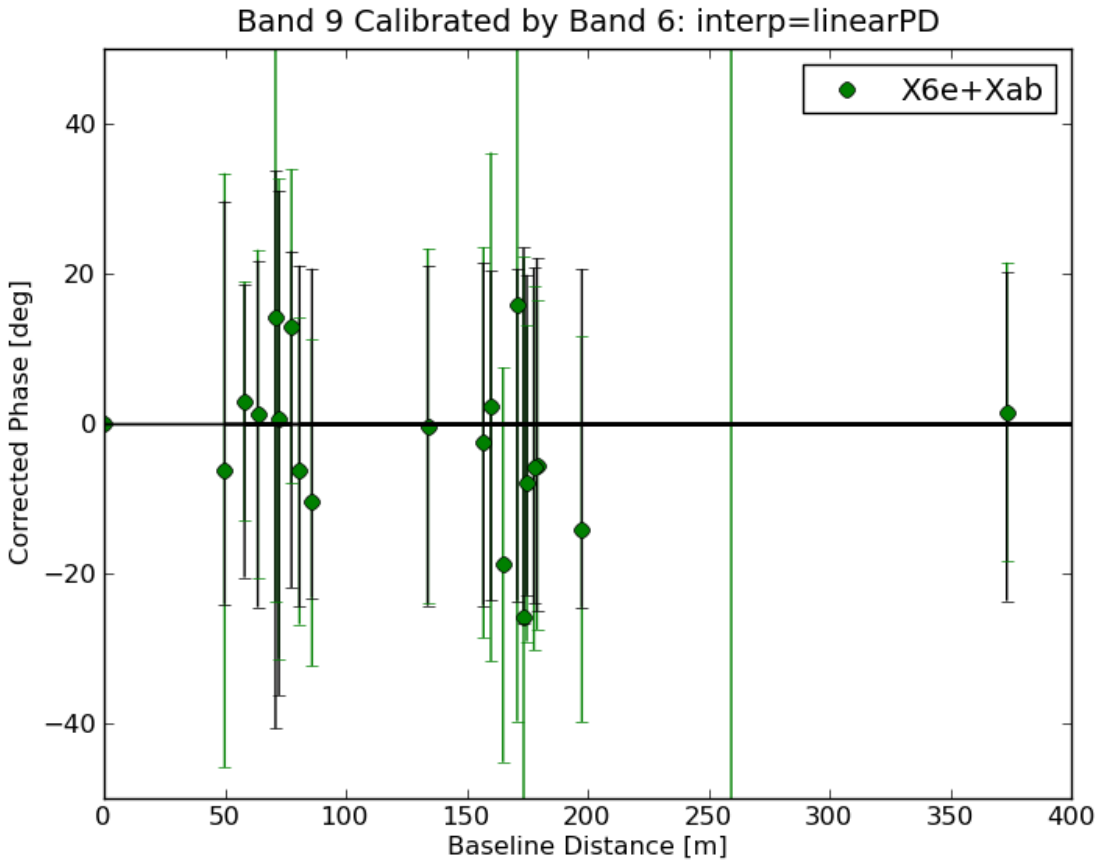

Figure 32: Mean corrected phase for each antenna as a function of baseline distance for the observation X6e+Xab. See the caption to Figure 31 for a full description.

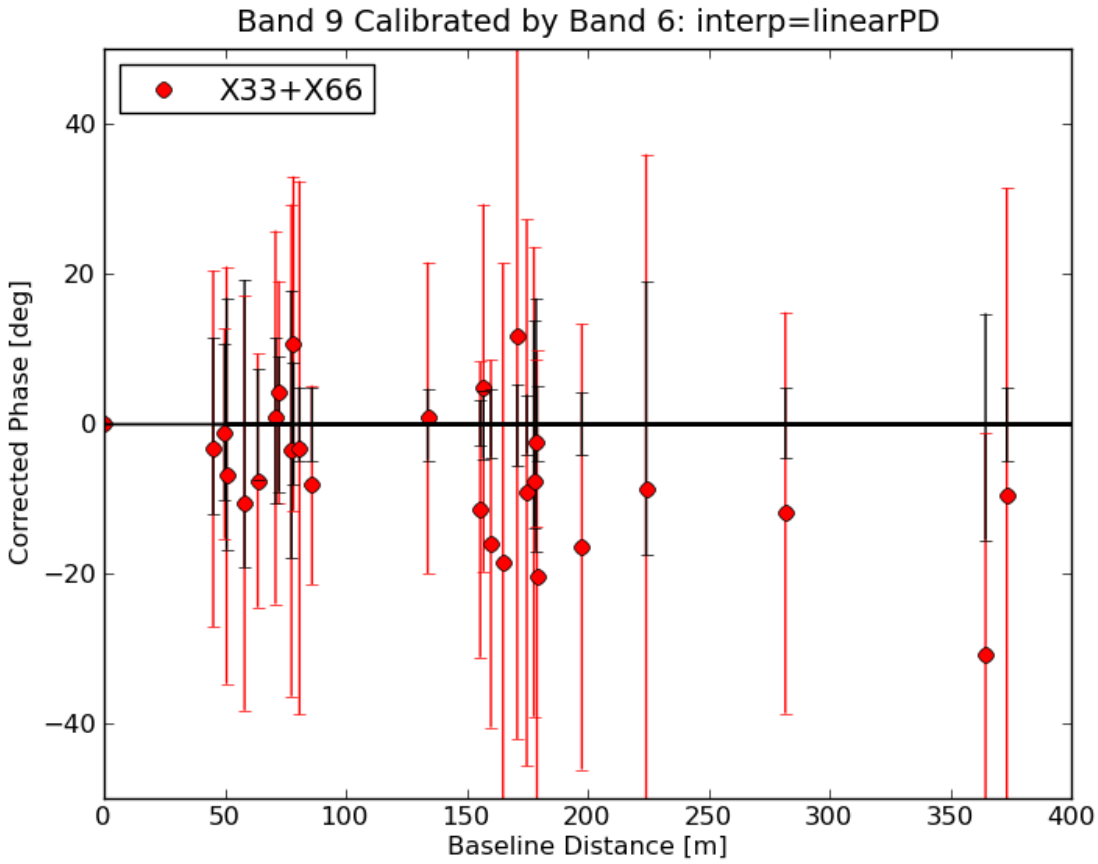

Figure 33: Mean corrected phase for each antenna as a function of baseline distance for the observation X6e+Xab. See the caption to Figure 31 for a full description.

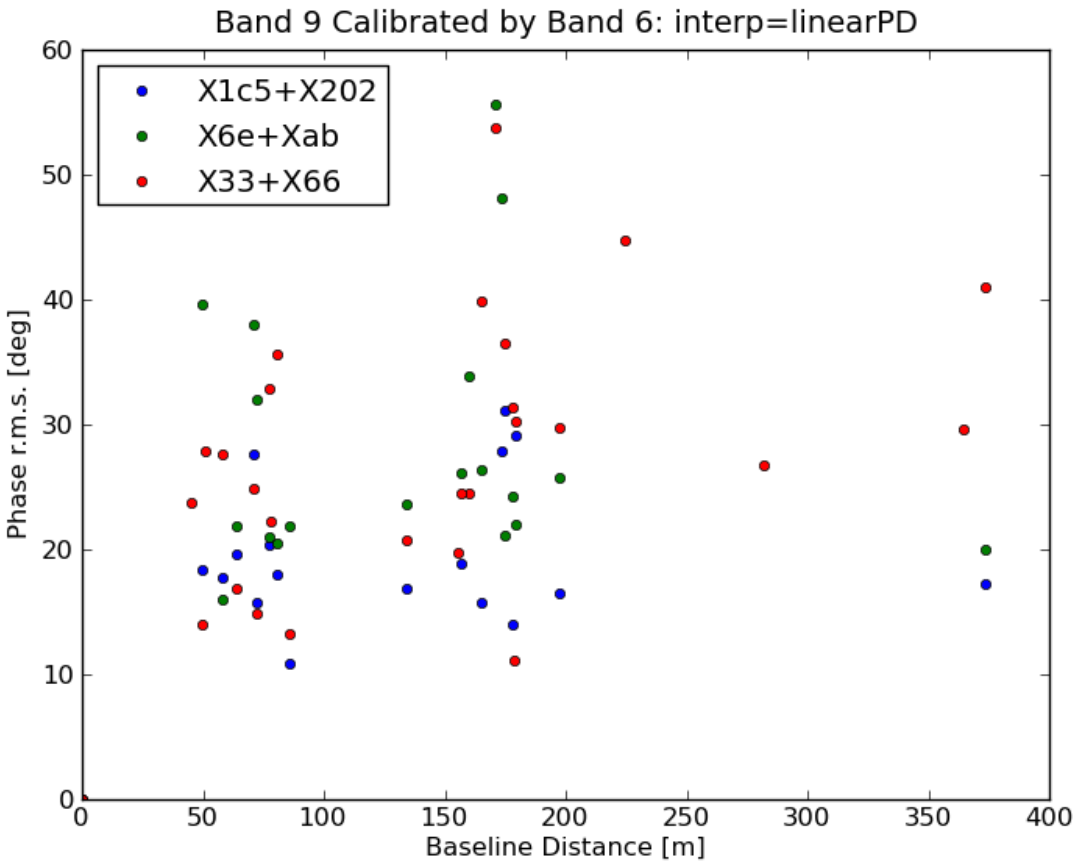

Figure 34: Corrected phase r.m.s. for each antenna as a function of baseline distance for all Band 6/Band 9 observations as labeled, using interp='linearPD' (scaling of the solutions by the frequency ratio).

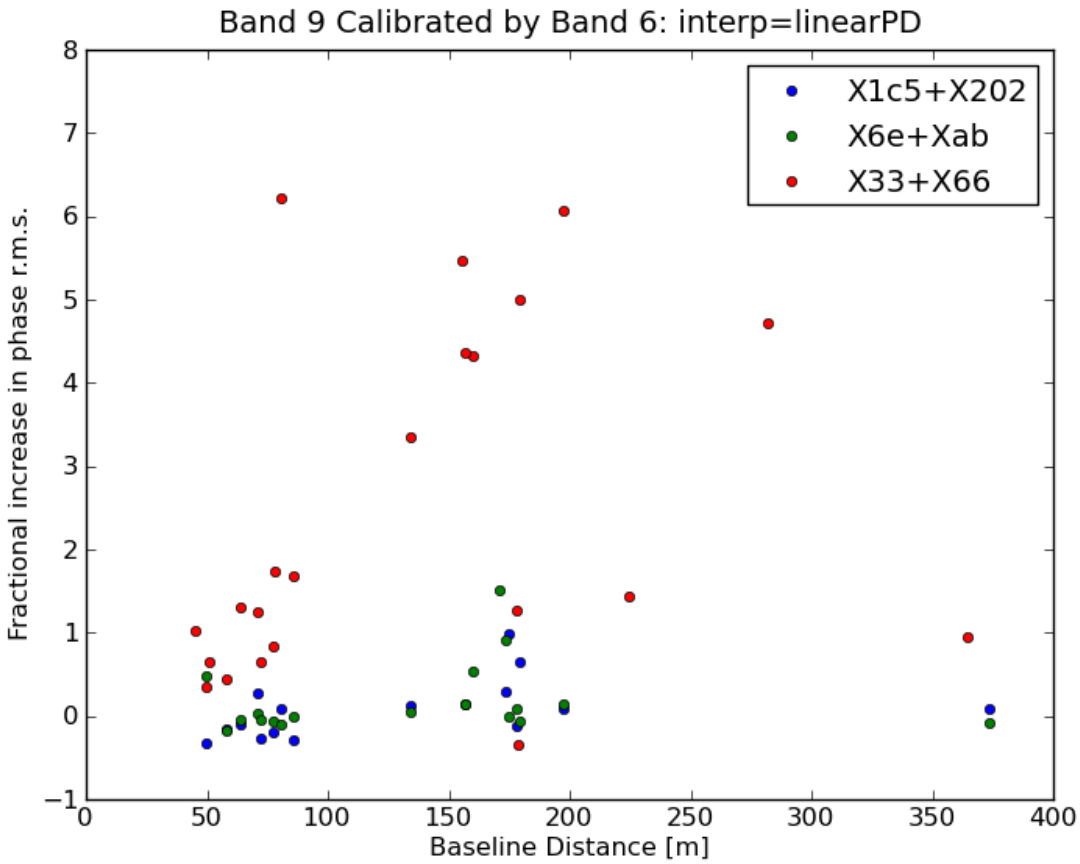

Figure 35: Fractional increase in the corrected phase r.m.s. for each antenna as a function of baseline distance for all Band 6/Band 9 observations as labeled, using interp='linearPD' (scaling of the solutions by the frequency ratio).